(will be inserted by the editor)

An investigation of a nonlocal hyperbolic model for self-organization of biological groups

Razvan C Fetecau · Raluca Eftimie

Received: date / Accepted: date

Abstract In this article, we introduce and study a new nonlocal hyperbolic model for the formation and movement of animal aggregations. We assume that the nonlocal attractive, repulsive, and alignment interactions between individuals can influence both the speed and the turning rates of group members. We use analytical and numerical techniques to investigate the effect of these nonlocal interactions on the long-time behavior of the patterns exhibited by the model. We establish the local existence and uniqueness and show that the nonlinear hyperbolic system does not develop shock solutions (gradient blow-up). Depending on the relative magnitudes of attraction and repulsion, we show that the solutions of the model either exist globally in time or may exhibit finite-time amplitude blow-up. We illustrate numerically the various patterns displayed by the model: dispersive aggregations, finite-size groups and blow-up patterns, the latter corresponding to aggregations which may collapse to a point. The transition from finite-size to blow-up patterns is governed by the magnitude of the social interactions and the random turning rates. The presence of these types of patterns and the absence of shocks are consequences of the biologically relevant assumptions regarding the form of the speed and the turning rate functions, as well as of the kernels describing the social interactions.

AMS subject classification: 92D25, 92D50, 35L65

Keywords biological aggregations · nonlinear hyperbolic systems · nonlocal interactions · alignment · blow-up

1 Introduction

The complex spatial and spatiotemporal patterns observed in animal aggregations have always fascinated the scientists, who tried to understand their formation, as well as their long-time behavior [1,2,3,4]. Examples of such patterns are offered by schooling fish, foraging herds of ungulates, swarming insects and zigzagging flocks of birds. These patterns range from relatively loose groups, as observed in certain schools of fish [5] or swarms of insects [6] to extremely high-density animal aggregations. An example of the latter pattern is offered by [7], who reported how under the threat of predation, a school of fish collapsed into a very tight ball which became almost motionless. Investigations in [8] on the other hand, account for a rapidly moving compact mass of about one cubic foot, formed of approximately 7500 fish.

The reasons for which insects and animals aggregate are quite well understood. For example, belonging to a group improves their chances of survival, of finding mates or food. However, limited information exists regarding the specific mechanisms that lead to the formation of the diverse spatial and spatiotemporal group patterns observed in nature. In particular, it is unclear how individual movement decisions and signal reception mechanisms integrate and also what triggers the observed transitions between patterns.

For the past fifty years, mathematical models have been used extensively to reproduce, investigate, and understand some of the biological mechanisms behind these self-organized animal aggregation patterns. These models fall into two categories: Lagrangian models, where the movement of individual organisms is governed

R. Fetecau
Department of Mathematics, Simon Fraser University, Burnaby, BC V5A 1S6, Canada
Tel.: 778-782-3335
E-mail: van@math.sfu.ca

R. Eftimie
Department of Mathematics and Statistics, McMaster University, Hamilton, ON L8S 4K1, Canada

by a set of decision rules (e.g., [4,9,10,11], and the references therein), and Eulerian models, which focus on the average density of individuals (e.g., [12,2,13], and the references therein). This article concerns only the latter type. The Eulerian approach casts the problem as an evolution equation for the population density field. The various model equations suggested in the literature are of either parabolic [14,2,15,16,13] or hyperbolic [17,12,18] types. Depending on the social interactions between group members, the Eulerian models can also be classified into local and nonlocal types. For local models [19,12,20] the immediate neighbors or local environmental effects are important, while for nonlocal ones [14,17,2,18,13] the distant individuals or nonlocal factors play the dominant role. The nonlocal parabolic models are usually described by advection-diffusion equations, and assume that the nonlocal attractive and repulsive interactions influence the speeding-up/slowing-down behavior [2,13]. The hyperbolic models, on the other hand, generally focus on the turning behavior, which can be described by nonlocal alignment [18], as well as nonlocal attractive and repulsive terms [17,21].

The hyperbolic aggregation models have shown very rich spatial and spatiotemporal patterns. Most of these are finite density aggregations, such as stationary and traveling pulses, ripples, zigzags, and traveling trains [21, 12]. In addition, hyperbolic models support blow-up solutions, where the density increases steeply and the group collapses into one point [19,22].

A very interesting and intriguing aspect of animal aggregations [23] is the dynamical transition between different patterns. A recent study [24] uses bifurcation methods along with linear and weakly nonlinear analysis to investigate the biological mechanisms that lead to such changes in a nonlocal hyperbolic model. Other works show that the use of different types of communication mechanisms [21], as well as the change in the magnitudes of the social interactions [17,24] or the group density [13] can cause transitions between patterns. All these results however refer to transitions between patterns with relatively low amplitudes, corresponding to loose aggregations and omit the cases where species form very dense groups [7,8]. In this paper, we address this issue and investigate the transition between high and low-density patterns by looking into possible biological mechanisms that may cause or inhibit the formation of high densities or blow-up in animal aggregations.

This article introduces and investigates an extension of a nonlocal hyperbolic model for biological aggregations derived in [17] and further investigated in [21,24]. The model from [17] consists in the following system of conservation laws for the right and left moving densities of individuals u^+ and u^-, respectively:

$$\partial_t u^+ + \partial_x(\gamma u^+) = -\lambda^+[u^+,u^-]u^+ + \lambda^-[u^+,u^-]u^-, \tag{1a}$$

$$\partial_t u^- - \partial_x(\gamma u^-) = \lambda^+[u^+,u^-]u^+ - \lambda^-[u^+,u^-]u^-. \tag{1b}$$

Here γ is a constant speed, and λ^+ (λ^-) denote the turning rates of the individuals that were initially moving to the right (left) and then turn to change direction. The main merit of model (1) is that it takes into account *all* three social interactions (attraction, repulsion and alignment) that govern the response of an individual to signals perceived from its neighbors. The three social interactions are modeled by nonlocal terms that enter in the expressions of the turning rates $\lambda^\pm$. The functional dependence of $\lambda^\pm$ on the nonlocal social interactions will be made precise in the next section.

Model (1) proved to be very versatile, by capturing a very complex range of behaviors observed in biological systems. Examples of such patterns are stationary and traveling groups, zigzags, breathers, or ripples [21]. Some of these solutions apparently emerge only as a result of interactions between all three social forces (attraction, repulsion and alignment). Moreover, the transition between some of these finite-density patterns are caused by changes in the magnitudes of the social forces [24].

A shortcoming of the model (1) is the assumption that individuals move at a constant speed γ. The assumption is not realistic, since many of the organisms observed in nature adapt their speed as a result of interactions with conspecifics [1,25]. In this article, we extend the model by assuming that the individuals speed-up or slow-down as a result of attraction towards other individuals far away, or repulsion from individuals near-by. We replace the constant γ by density-dependent speeds $\Gamma^\pm$ that incorporate nonlocal attraction and repulsion effects, while keeping the right-hand-side the same — see system (2) in Section 2. The assumption of nonlocal density-dependent speeds is in the spirit of other parabolic [2,13] and hyperbolic models [16,26,22] available in the literature. Note that a hyperbolic model that incorporates both density-dependent speeds and turning rates also appears in [19] in the context of 1-D chemotaxis. However, the model we propose in this article is the first hyperbolic model with density-dependent speeds which assumes that all social interactions are nonlocal, and all might contribute to the complex patterns displayed by the hyperbolic system.

The nonlocal interaction terms in (1) are modeled using kernel functions. Another shortcoming of the model (1) from [17] is the assumption that the attractive and repulsive kernels are continuous at the origin. This implies that when individuals are close to each other, the repulsion force between them is very weak. To address this biological inaccuracy, some mathematical models (both Lagrangian [27] and Eulerian [26,22]) consider attractive-repulsive functions that are discontinuous at the origin. In the present article we follow a similar approach and investigate the patterns that can be obtained with discontinuous kernels.

The present article contains an analytical and numerical study of the extension of the hyperbolic model (1). Since the speeds are density dependent, one might expect shock formation through slope steepening, as in nonlinear conservation laws. Shock formation is not an issue for system (1), where the speeds are constant. In fact, provided the turning rates are bounded (and this is an assumption that we do make), (1) behaves like a linear system. A regular solution to (1) exists globally in time [24]. The analysis for the hyperbolic system with nonlocal density-dependent speeds is more intricate. We show that the solutions of this system do not exhibit shock formation as long as their amplitude stays bounded. Note that formation of shocks was observed in models for human or human-related self-organized aggregations [28,29,30].

Our extended model displays finite-size stationary aggregations (as seen for example in resting herds of ungulates [41]), as well as finite-time blow-up patterns which may correspond for instance to the collapsing behavior seen in certain schools of fish [7,8]. From a mathematical point of view, the amplitude blow-up is caused by the discontinuity of the interaction kernel that introduces a quadratic nonlinearity in the characteristic equations. The original model (1) cannot exhibit such patterns. Amplitude finite-time blow-up is a common phenomenon displayed by parabolic [31,32] and hyperbolic models [19] for chemotaxis. In these models, the blow-up is due to the chemotactic communication that can cause bacteria to aggregate in a delta function, or to form very dense but finite-size aggregations [19]. In contrast, in our model the blow-up is caused by the assumption that on very close distances, the repulsion-attraction force which influences the speeding behavior is strong.

Finally, the present article sheds new light on the factors that influence the transition between low and high density aggregation patterns. We show that the collapse of a group can be prevented by increasing the rate at which the individuals turn randomly. Also, the random turning rates have a great effect on the looseness of aggregations. These facts suggest that changes in the turning rates represent an important mechanism that leads to the transition between patterns, in particular from blow-up to finite-density aggregations.

The structure of the article is as follows. In Section 2, we describe the new hyperbolic model which incorporates both nonlocal attractive and repulsive speeds, and nonlocal turning rates. Then, in Section 3, we show that the model cannot display shock solutions. In Section 4, we investigate the global existence of finite-size aggregations, as well as the finite-time blow-up of solutions. Section 5 contains various numerical studies which support and complement the analytical results regarding the possible types of aggregations. A summary of the results is presented in Section 6. The local existence and uniqueness of solutions is deferred to the Appendix.

2 A model for aggregation of species

In this section, we introduce the new nonlocal hyperbolic model that generalizes system (1) derived in [17] to describe the formation and movement of animal groups. As mentioned in the introduction, the model from [17] assumes that individuals move at a constant speed, and turn to approach, to avoid, or to align with their neighbors. The social interactions governing these behaviors are described by nonlocal terms. However, organisms do not always move at a constant speed, as they speed-up or slow-down to approach their neighbors, or to avoid collisions [1,25]. Therefore, we extend the model proposed in [17] to incorporate the speeding-up and slowing-down behaviors which result from attractive and repulsive interactions. Following the approach in [2,13], we assume that these interactions are also nonlocal.

The new model is described by equations

$$\partial_t u^+ + \partial_x \left(\Gamma^+[u^+,u^-]u^+ \right) = -\lambda^+[u^+,u^-]u^+ + \lambda^-[u^+,u^-]u^- \tag{2a}$$

$$\partial_t u^- - \partial_x \left(\Gamma^-[u^+,u^-]u^- \right) = \lambda^+[u^+,u^-]u^+ - \lambda^-[u^+,u^-]u^-, \tag{2b}$$

with an initial condition $u^\pm(x,0) = u_0^\pm(x)$, $x \in \mathbb{R}$. These equations describe the evolution of densities of right-moving (u^+) and left-moving (u^-) individuals of a self-organizing animal aggregation. Here, $\Gamma^\pm[u^+,u^-]$ and $\lambda^\pm[u^+,u^-]$ denote the density-dependent speeds and the turning rates, respectively.

We assume that the speeds $\Gamma^\pm[u^+,u^-]$ have the form

$$\Gamma^+[u^+,u^-] = \gamma(1 + f(K * u)), \tag{3a}$$

$$\Gamma^-[u^+,u^-] = \gamma(1 - f(K * u)), \tag{3b}$$

where $*$ denotes convolution. Here, f is a non-decreasing monotone function describing the effect of the social interactions on the speeding-up/slowing-down behaviors. The negative and positive signs in front of f suggest the opposite effect of these interactions on the speed of left-moving and right-moving individuals. The expression (3) for $\Gamma^\pm$ is quite general and it includes as special cases nonlocal velocities considered in other aggregation

models (various mathematical models [2,13,26,22] have the nonlocal velocities defined in terms of the identity function for instance). The constant $\gamma > 0$ is a base-line speed which characterizes the movement in the absence of any social interactions. Also,

$$u = u^+ + u^-$$

is the total population density, and the kernel

$$K(x) = -q_a K_a(x) + q_r K_r(x) \tag{4}$$

models attraction and repulsion interactions between individuals. The positive constants q_a and q_r represent the magnitudes of the attractive and repulsive interactions, respectively. We will discuss shortly the form of the attraction and repulsion kernels, K_a and K_r. Biologically relevant interaction kernels K are odd functions on the real line that typically have a discontinuity at the origin [1]. This discontinuity at the origin accounts for the strong repulsive interactions which act on very short spatial ranges. Therefore, in general, the jump at the origin is

$$[K] = K(0+) - K(0-) \neq 0,$$

where $K(0+)$ and $K(0-)$ represent the values of K as x approaches 0 with positive and negative values, respectively. Except for this jump, the kernel K is smooth everywhere in $\mathbb{R} \setminus \{0\}$, is integrable and decays to 0 at infinity. The oddness of K ensures that individuals exert equal and opposite forces on each other.

Early works on aggregation models [2] consider continuous kernels (i.e., $K(0) = 0$) of the form xe^{-x^2}. In [17], the kernels K_a and K_r are taken to be odd extensions of translated Gaussian functions defined on $(0, \infty)$. Both choices are not very realistic as they make the interaction forces to be very weak on short ranges. Other works [33,26,22] consider Morse interaction kernels of exponential type:

$$K(x) = \operatorname{sgn}(x) \left(-q_a e^{\frac{-|x|}{s_a}} + q_r e^{\frac{-|x|}{s_r}} \right), \tag{5}$$

where $s_{r,a}$ represent the widths of the attractive and repulsive interaction ranges. In this paper, we only consider exponential kernels of the form (5) and, for a biologically realistic case, assume that $s_r < s_a$. The magnitude of the interaction force at 0, $|q_r - q_a|$, could be small or large, depending on the relative sizes of q_a and q_r. See Figure 1(a)-(b) for plots of the kernel (5) when (a) $q_a < q_r$ and (b) $q_a > q_r$. The relative sizes of q_a and q_r prove to be very important in the subsequent analysis.

The turning rates $\lambda^{\pm}[u^+, u^-]$ are taken to be bounded, positive and monotone functions of the signals $y^{\pm}[u^+, u^-]$ perceived by individuals as a result of social interactions with neighbors:

$$\lambda^{\pm}[u^+, u^-] = a + b\, g(y^{\pm}[u^+, u^-]). \tag{6}$$

The constants a and b represent a base-line random turning rate and a biased turning rate, respectively. The function g is a bounded and increasing function on the real line and $y^{\pm}[u^+, u^-]$ are dimensionless functionals on the densities of right-moving (u^+) and left-moving (u^-) individuals.

We assume that the perceived signals $y^{\pm}[u^+, u^-]$ are in the form [17]

$$y^{\pm}[u^+, u^-] = y_r^{\pm}[u^+, u^-] - y_a^{\pm}[u^+, u^-] + y_{al}^{\pm}[u^+, u^-], \tag{7}$$

where $y_r^{\pm}$, $y_{al}^{\pm}$ and $y_a^{\pm}$ represent the repulsion, alignment and attraction terms that influence the likelihood of turning to the left ($+$) or to the right ($-$). Note that the repulsive and attractive terms have opposite effects.

The expressions for the interaction signals that we consider below are taken from [17] and we refer the reader to this work for a detail account on the modeling of these terms. For instance, an individual positioned at (x, t) that moves to the right ($+$) receives information from other individuals located to its right, at $x + z$, and to its left, at $x - z$. To model attraction and repulsion signals we consider all individuals $u(x + z)$ and $u(x - z)$ located ahead and behind, respectively, while for alignment we consider only individuals that move toward the considered individual, that is $u^-(x + z)$ and $u^+(x - z)$.

The repulsion and attraction signals have the expressions

$$y_{r,a}^{+}[u^+, u^-] = q_{r,a} \int_0^{\infty} K_{r,a}(z)(u(x + z, t) - u(x - z, t))dz, \tag{8a}$$

$$y_{r,a}^{-}[u^+, u^-] = q_{r,a} \int_0^{\infty} K_{r,a}(z)(u(x - z, t) - u(x + z, t))dz, \tag{8b}$$

where K_r and K_a are the repulsion and the attraction kernels, in the exponential form (see (4) and (5)).

[1] Our results include the case of continuous kernels, considered in some early models (e.g., [2]).

The alignment terms are given by

$$y_{al}^{+}[u^{+},u^{-}] = q_{al}\int_{0}^{\infty} K_{al}(z)(u^{-}(x+z,t)-u^{+}(x-z,t))dz, \tag{9a}$$

$$y_{al}^{-}[u^{+},u^{-}] = q_{al}\int_{0}^{\infty} K_{al}(z)(u^{+}(x-z,t)-u^{-}(x+z,t))dz, \tag{9b}$$

where K_{al} represents the alignment kernel, defined on $(0,\infty)$, and q_{al} measures the magnitude of the alignment. In this paper we consider the same alignment kernel K_{al} used in [17], given by a Gaussian function (see Figure 1 (c)):

$$K_{al}(x) = \frac{1}{\sqrt{2\pi m_{al}^{2}}}\exp\left(-(x-s_{al})^{2}/(2m_{al}^{2})\right), \quad x\in[0,\infty). \tag{10}$$

Here $m_{al} = s_{al}/8$ represents the width of the alignment kernel, while s_{al} represents the length of the alignment range. The constant m_{al} is chosen such that the support of more than 98% of the mass of the kernel is inside the interval $[0,\infty)$.

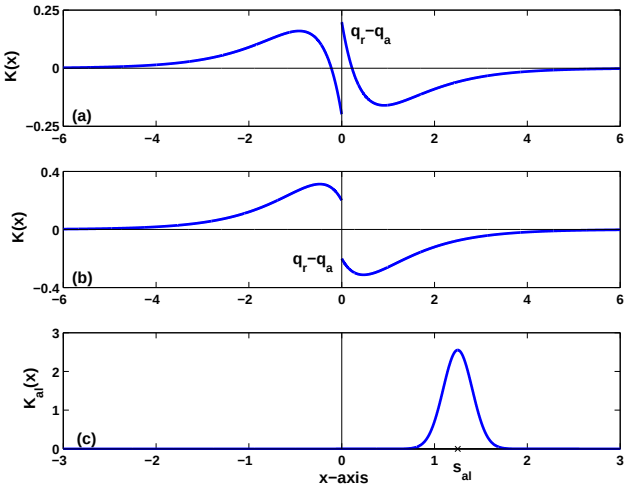

Fig. 1 Examples of kernels used for social interactions. These kernels describe how signals from different distances are weighted. (a)-(b) The interaction kernel given by (5). In (a) repulsion is stronger than attraction ($q_a = 0.8$, $q_r = 1$), while in (b) the situation is reversed ($q_a = 1$, $q_r = 0.8$). In both cases, $s_a = 1$, $s_r = 0.5$. (c) Translated Gaussian kernel for alignment — see (10), where $s_{al} = 1.25$ and $m_{al} = s_{al}/8$. Note that all these parameter values are used in the numerics section.

The model proposed in [17] has the same form as (2), except that the speeds $\Gamma^{\pm}$ are simply taken to be constant ($=\gamma$). The new model (2) is more realistic, as it includes nonlocal interaction terms in the expressions (3) for the speeds $\Gamma^{\pm}$.

In the following sections, we investigate analytically and numerically the different types of patterns displayed by the nonlocal hyperbolic model (2). In particular, we start by exploring the possibility of having shocks (i.e., finite aggregations whose gradient blows up in finite time). These types of patterns are quite common in models describing human and human-related aggregations, such as human traffic models (e.g., [28,30]), and are somewhat expected from nonlinear hyperbolic systems such as (2).

3 Amplitude control guarantees no shock formation

In this section, we start investigating the different types of solutions of (2). To this end, we assume that system (2) has a local classical solution (the existence of such a solution is proved in the Appendix), and we investigate whether or not the system can produce shocks, that is discontinuities in the first derivatives. This is a very

natural question to ask, since the left-hand sides of the equations (2) are in conservation law form, and the shock formation in hyperbolic conservation laws is a well-known mechanism for breakdown of solutions [34,35]. Note however, that the fluxes in (2) are products of the densities u^+, u^- with their corresponding velocities, the latter being described by convolutions with the former. This particular structure of the flux vector fundamentally changes the behavior of solutions of (2) as compared to solutions of hyperbolic conservation laws, at least in as far as shock formation is concerned.

To simplify the presentation of the results from this section and the Appendix, we assume that the perceived signals $y^\pm$ from (7) have only an alignment component, i.e. $y^\pm[u^+,u^-] = y_{al}[u^+,u^-]$. All the arguments from this section, as well as those referring to local existence and uniqueness from the Appendix can be trivially adapted to include attraction and repulsion terms in $y^\pm$.

In the following, we show that assuming that there is an a priori bound on the magnitude of the solution (u^+,u^-), then no shocks can form in finite time. In other words, the formation of shocks as typical to hyperbolic systems should not be considered as a possible finite time blow-up criteria for system (2). This is a consequence of the assumptions made on the functions describing the speed ($f(x)$) and the turning rates ($g(x)$). The finite time blow-up may occur due to the unbounded increase of the solution (u^+,u^-) itself, as we show later, in Section 4.

To start, let us make the assumption

$$\max\left(\|u^+(\cdot,t)\|_\infty, \|u^-(\cdot,t)\|_\infty\right) \leq M, \qquad \text{for } 0 \leq t \leq T. \tag{11}$$

We are interested in showing that no shocks can form up to time T.

Note that u^+ and u^- are supposed to be non-negative functions, as they represent densities of individuals. It is a simple exercise to show that system (2) preserves the non-negativity of the initial data, that is

$$u^+(\cdot,t) \geq 0, \quad u^-(\cdot,t) \geq 0,$$

provided

$$u_0^+(\cdot) \geq 0, \quad u_0^-(\cdot) \geq 0.$$

Hence, the boundedness assumption (11) can also be written as

$$0 \leq u^+(x,t), u^-(x,t) \leq M, \qquad \text{for all } x \in \mathbb{R},\, t \in [0,T].$$

Assumptions on K, K_{al}, f and g. Suppose that the kernel K is given by

$$K(x) = \begin{cases} K^-(x) & x < 0 \\ K^+(x) & x > 0, \end{cases}$$

where the components K^- and K^+ are differentiable on $(-\infty,0)$ and $(0,\infty)$, respectively [2]. Note that the kernel (5) can be written in this form. Then, one can define the piecewise derivative of K by

$$K^{(1)}(x) = \begin{cases} (K^-)'(x) & x < 0 \\ (K^+)'(x) & x > 0. \end{cases} \tag{12}$$

Similarly, one can define the 2nd and 3rd order piecewise derivatives $K^{(2)}$ and $K^{(3)}$.

We make the following assumptions on the kernels K and K_{al}, and on the functions f and g used in defining $\Gamma^\pm$ and $\lambda^\pm$:

- (P1) The kernel K is odd, has a discontinuity at the origin, but is smooth everywhere in $\mathbb{R} \setminus \{0\}$.
- (P2) The kernel K and its piecewise derivatives $K^{(1)}$, $K^{(2)}$ and $K^{(3)}$ are integrable.
- (P3) The kernel K_{al} is bounded.
- (P4) f and g are non-decreasing functions on the real line that have uniformly bounded derivatives up to the 3rd and 2nd orders, respectively. The function g is also assumed to be bounded.

[2] Since K is also assumed to be odd, we have in fact $K^-(x) = -K^+(-x)$, for all $x < 0$

Typical choices of the kernels K and K_{al} (as seen in [17,22] for instance) satisfy properties (P1)-(P3). In [17], the authors take the function g to be given by

$$g(x) = 0.5 + 0.5\tanh(x - x_0), \tag{13}$$

with the constant x_0 chosen such that $g(0) \ll 1$. In the numerical results presented in Section 5 we take f to be the hyperbolic tangent, $f(x) = \tanh(x)$. Another option would be to simply take f be the identity, as in other works on aggregation models [2,13,26,22]. These choices of f and g satisfy assumption (P4).

L^1-control of u^+ and u^-. Add (2a) and (2b), and then integrate over $\mathbb{R}$. The second terms in the left-hand-sides render 0, and the right-hand-sides cancel each other. We get

$$\frac{d}{dt}(\|u^+\|_{L^1} + \|u^-\|_{L^1}) = 0.$$

Hence,

$$\|u(\cdot,t)\|_{L^1} = \|u_0\|_{L^1}, \tag{14}$$

where $u_0 = u_0^+ + u_0^-$. Note that this estimate does not use assumption (11).

L^1-control of u_x^+ and u_x^-. Take the derivative with respect to x in (2a), multiply by $\operatorname{sgn}(u_x^+)$ and integrate over the x-domain. The left-hand-side of the resulting equation is

$$\frac{d}{dt}\int |u_x^+|dx + \int \left(\Gamma_x^+ u^+\right)_x \operatorname{sgn}(u_x^+)dx + \int \left(\Gamma^+ u_x^+\right)_x \operatorname{sgn}(u_x^+)dx.$$

The last term in this sum renders 0. Therefore, we get

$$\frac{d}{dt}\int |u_x^+|dx \le \int \left(|\Gamma_{xx}^+||u^+| + |\Gamma_x^+||u_x^+| + |(\lambda^+ u^+)_x| + |(\lambda^- u^-)_x|\right) dx. \tag{15}$$

Now, we compute Γ_x^+ and Γ_{xx}^+. From (3a),

$$\begin{aligned}\Gamma_x^+(x,t) &= \gamma f'(K*u(x,t))\frac{\partial}{\partial x}(K*u)(x,t)\\ &= \gamma f'(K*u(x,t))\left([K]u(x,t) + K^{(1)}*u(x,t)\right).\end{aligned} \tag{16}$$

Recall that $K^{(1)}$ denotes the piecewise derivative of K — see (12). The calculation of Γ_{xx}^+ yields

$$\begin{aligned}\Gamma_{xx}^+(x,t) = &\\ &\gamma f''(K*u(x,t))\left([K]u(x,t) + K^{(1)}*u(x,t)\right)^2 + \gamma f'(K*u(x,t))\left([K]u_x(x,t) + K^{(2)}*u(x,t)\right),\end{aligned}$$

where we used the fact that $K^{(1)}$ is continuous. where we used the fact that $K^{(1)}$ is continuous. This property follows from the fact that K is odd and hence, $(K^-)'(x) = (K^+)'(-x)$, for all $x < 0$. Therefore there is no jump of $K^{(1)}$ at 0.

Using the fact that f' and f'' are bounded functions, the following estimates become readily available [3]

$$\|\Gamma_x^+(\cdot,t)\|_{L^\infty} \le C\left([K] + \|K^{(1)}\|_{L^1}\right)\|u(\cdot,t)\|_{L^\infty}, \tag{17}$$

$$\begin{aligned}\|\Gamma_{xx}^+(\cdot,t)\|_{L^1} &\le C(\|[K]u(\cdot,t) + K^{(1)}*u(\cdot,t)\|_{L^\infty}\|[K]u(\cdot,t) + K^{(1)}*u(\cdot,t)\|_{L^1}\\ &\quad + C[K]\|u_x(\cdot,t)\|_{L^1} + C\|K^{(2)}*u(\cdot,t)\|_{L^1}\\ &\le C\left([K] + \|K^{(1)}\|_{L^1}\right)^2\|u(\cdot,t)\|_{L^\infty}\|u(\cdot,t)\|_{L^1}\\ &\quad + C[K]\|u_x(\cdot,t)\|_{L^1} + C\|K^{(2)}\|_{L^1}\|u(\cdot,t)\|_{L^\infty}.\end{aligned}$$

[3] Recall the following basic properties of convolutions

$$\begin{aligned}\|f*g\|_{L^\infty} &\le \|f\|_{L^1}\|g\|_{L^\infty}, &&\text{for } f \in L^1(\mathbb{R}), g \in L^\infty(\mathbb{R})\\ \|f*g\|_{L^1} &\le \|f\|_{L^1}\|g\|_{L^1}, &&\text{for } f, g \in L^1(\mathbb{R})\end{aligned}$$

We use the symbols C, C_1, C_2 to denote generic constants. The kernels $K^{(1)}$, $K^{(2)}$ are integrable, and $\|u(\cdot,t)\|_{L^\infty}$, $\|u(\cdot,t)\|_{L^1}$ are bounded for $0 \le t \le T$. Hence, the last sequence of inequalities shows that

$$\|\Gamma^+_{xx}(\cdot,t)\|_{L^1} \le C_1 + C_2\|u_x(\cdot,t)\|_{L^1}, \tag{18}$$

for some constants C_1 and C_2.

To estimate the terms $\|(\lambda^+u^+)_x\|_{L^1}$ and $\|(\lambda^-u^-)_x\|_{L^1}$ in the right-hand-side of (15), we have to calculate λ^+_x and λ^-_x. From (6) and (9a) we compute:

$$\lambda^+_x = bg'(y^+)\left(q_{al}\int_0^\infty K_{al}(z)(u^-_x(x+z,t) - u^+_x(x-z,t))dz\right).$$

From here, using the fact that g' and the kernel K_{al} are bounded, we derive

$$\|\lambda^+_x\|_{L^\infty} \le C\left(\|u^+_x\|_{L^1} + \|u^-_x\|_{L^1}\right), \tag{19}$$

for some constant C.

Then

$$\|(\lambda^+u^+)_x\|_{L^1} \le \|\lambda^+_x\|_{L^\infty}\|u^+\|_{L^1} + \|\lambda^+\|_{L^\infty}\|u^+_x\|_{L^1}.$$

Using the boundedness of λ^+ and the L^1-control on u^+, the last two inequalities imply that

$$\|(\lambda^+u^+)_x\|_{L^1} \le C\left(\|u^+_x\|_{L^1} + \|u^-_x\|_{L^1}\right). \tag{20}$$

A similar estimate holds for $\|\left(\lambda^-u^-\right)_x\|_{L^1}$.

Finally, return to (15) to derive

$$\begin{aligned}\frac{d}{dt}\int|u^+_x|dx &\le \|\Gamma^+_{xx}\|_{L^1}\|u^+\|_{L^\infty} + \|\Gamma^+_x\|_{L^\infty}\|u^+_x\|_{L^1} + \|(\lambda^+u^+)_x\|_{L^1} + \|(\lambda^-u^-)_x\|_{L^1}\\ &\le C_1 + C_2\left(\|u^+_x\|_{L^1} + \|u^-_x\|_{L^1}\right),\end{aligned} \tag{21}$$

for some constants C_1, C_2. For the last inequality we used (17), (18), (20), and the assumption (11).

Clearly a similar estimate can be derived for u^-. By adding them, we obtain

$$\frac{d}{dt}(\|u^+_x\|_{L^1} + \|u^-_x\|_{L^1}) \le C_1 + C_2(\|u^+_x\|_{L^1} + \|u^-_x\|_{L^1}).$$

Gronwall's lemma gives now L^1-control of the gradients of u^+ and u^-, for as long as the L^∞-norm of the solution is controlled.

L^1-control of u^+_{xx} and u^-_{xx}. Here, we show that $\|u^+_{xx}\|_{L^1}$ and $\|u^-_{xx}\|_{L^1}$ do not blow-up in finite time. The Sobolev embedding $W^{1,1}(\mathbb{R}) \subset L^\infty(\mathbb{R})$ then ensures that $\|u^+_x\|_{L^\infty}$ and $\|u^-_x\|_{L^\infty}$ stay bounded, and therefore no shocks form.

Take a double derivative with respect to x in (2a), multiply by $\operatorname{sgn}(u^+_{xx})$ and integrate over the x-domain. The left-hand-side of the resulting equation is

$$\frac{d}{dt}\int|u^+_{xx}|dx + \int\left(\Gamma^+_{xx}u^+ + 2\Gamma^+_x u^+_x\right)_x\operatorname{sgn}(u^+_{xx})dx + \int\left(\Gamma^+u^+_{xx}\right)_x\operatorname{sgn}(u^+_{xx})dx.$$

The integration of the last terms yields 0. Therefore,

$$\frac{d}{dt}\int|u^+_{xx}|dx \le \int\left(|\Gamma^+_{xxx}||u^+| + 3|\Gamma^+_{xx}||u^+_x| + 2|\Gamma^+_x||u^+_{xx}| + |(\lambda^+u^+)_{xx}| + |(\lambda^-u^-)_{xx}|\right)dx. \tag{22}$$

The second term in the right-hand-side can be estimated immediately:

$$\begin{aligned}\|\Gamma^+_{xx}u^+_x\|_{L^1} &\le \|\Gamma^+_{xx}\|_{L^1}\|u^+_x\|_{L^\infty}\\ &\le C\|u^+_{xx}\|_{L^1},\end{aligned} \tag{23}$$

where we used the embedding of $W^{1,1}(\mathbb{R})$ into $L^\infty(\mathbb{R})$ to bound $\|u^+_x\|_{L^\infty}$ by $\|u^+_{xx}\|_{L^1}$, and (18) and the previous results to bound $\|\Gamma^+_{xx}\|_{L^1}$ by a constant C that depends on T.

For the third term we use (17) to get

$$\|\Gamma^+_x u^+_{xx}\|_{L^1} \le C\|u^+_{xx}\|_{L^1}. \tag{24}$$

To estimate the first term, we need to calculate Γ^+_{xxx}:

$$\begin{aligned}\Gamma^+_{xxx} = &\gamma f'''(K*u(x,t))\left([K]u(x,t)+K^{(1)}*u(x,t)\right)^3\\ &+3\gamma f''(K*u(x,t))\left([K]u(x,t)+K^{(1)}*u(x,t)\right)\left([K]u_x(x,t)+K^{(2)}*u(x,t)\right)\\ &+\gamma f'(K*u(x,t))\left([K]u_{xx}(x,t)+[K^{(2)}]u(x,t)+K^{(3)}*u(x,t)\right),\end{aligned}$$

Using the boundedness of f', f'' and f''', the integrability of $K^{(1)}$, $K^{(2)}$ and $K^{(3)}$, and the control of $\|u\|_{L^\infty}$, $\|u\|_{L^1}$, and $\|u_x\|_{L^1}$ on $[0,T]$, it is easy to show that

$$\|\Gamma^+_{xxx}\|_{L^1} \le C_1 + C_2\|u_{xx}\|_{L^1},$$

where the constants C_1 and C_2 may depend on the final time T. This implies a bound on the first term in the right-hand-side of (22):

$$\begin{aligned}\|\Gamma^+_{xxx}u^+\|_{L^1} &\le \|\Gamma^+_{xxx}\|_{L^1}\|u^+\|_{L^\infty}\\ &\le C_1 + C_2(\|u^+_{xx}\|_{L^1}+\|u^-_{xx}\|_{L^1}).\end{aligned} \tag{25}$$

Finally, we estimate the terms $\|(\lambda^+u^+)_{xx}\|_{L^1}$ and $\|(\lambda^-u^-)_{xx}\|_{L^1}$ from the right-hand-side of (22). To this end, we calculate λ^+_{xx}:

$$\begin{aligned}\lambda^+_{xx} = &bg''(y^+)\left(q_{al}\int_0^\infty K_{al}(z)(u^-_x(x+z)-u^+_x(x-z))dz\right)^2\\ &+bg'(y^+)\left(q_{al}\int_0^\infty K_{al}(z)(u^-_{xx}(x+z)-u^+_{xx}(x-z))dz\right).\end{aligned}$$

Using the boundedness of g', g'' and K_{al}, as well as the L^1-control of u^+_x and u^-_x derived above, we get

$$\|\lambda^+_{xx}\|_{L^\infty} \le C_1 + C_2(\|u^+_{xx}\|_{L^1}+\|u^-_{xx}\|_{L^1}).$$

Then, from

$$\|(\lambda^+u^+)_{xx}\|_{L^1} \le \|\lambda^+_{xx}\|_{L^\infty}\|u^+\|_{L^1} + 2\|\lambda^+_x\|_{L^\infty}\|u^+_x\|_{L^1} + \|\lambda^+\|_{L^\infty}\|u^+_{xx}\|_{L^1},$$

sing (19), the boundedness of λ^+, and the L^1-control on u^+ and u^+_x, we derive

$$\|(\lambda^+u^+)_{xx}\|_{L^1} \le C_1 + C_2\left(\|u^+_{xx}\|_{L^1}+\|u^-_{xx}\|_{L^1}\right). \tag{26}$$

A similar estimate holds for $\|\left(\lambda^-u^-\right)_{xx}\|_{L^1}$. Now return to (22), and use (23)-(26) to get

$$\frac{d}{dt}\int |u^+_{xx}|dx \le C_1 + C_2\left(\|u^+_{xx}\|_{L^1}+\|u^-_{xx}\|_{L^1}\right), \tag{27}$$

for some constants C_1, C_2.

Clearly a similar estimate can be derived for u^-. By adding them, we obtain

$$\frac{d}{dt}(\|u^+_{xx}\|_{L^1}+\|u^-_{xx}\|_{L^1}) \le C_1 + C_2(\|u^+_{xx}\|_{L^1}+\|u^-_{xx}\|_{L^1}).$$

Gronwall's lemma gives L^1-control of u^+_{xx} and u^-_{xx} and hence, L^∞-control of u^+_x and u^-_x . Therefore, no shocks can form as long as the solution (u^+,u^-) remains bounded, and this result can be stated as follows:

Theorem 31. *Consider system (2) with non-negative initial data $(u^+_0,u^-_0) \in W^{2,1}(\mathbb{R})\times W^{2,1}(\mathbb{R})$, and suppose that a classical solution exists in a short time interval [4]. Then, the solution $(u^+(\cdot,t),u^-(\cdot,t))$ stays in $W^{2,1}(\mathbb{R})\times W^{2,1}(\mathbb{R})$ for arbitrarily long times, as long as it remains bounded. In particular, the solution is of class C^1 and has bounded first order space derivatives (no shocks form).*

In summary, the assumptions made on this hyperbolic model ensure that the organisms do not collide with each other to create shocks (as observed in large human aggregations [30]). This happens independent on whether the organisms turn around under the effect of attractive or repulsive forces, as the results depend only on the the assumptions that the turning function g, as well as certain high order derivatives of f and g are bounded. However realistic these assumptions are, they cannot explain the animal stampede (i.e. mathematical shocks) observed for example in those large ungulate herds in Serengeti plains [36]. This stampede, which can be attributed to sudden changes in animal speed, could be explained by this hyperbolic model if, for example, the acceleration or the rate of turning around would approach infinite values.

[4] The local existence of a classical solution to (2) is shown in the Appendix.

4 Global existence for $[K] \geq 0$, possible finite-time blow-up for $[K] < 0$

We study the effect of the attractive and repulsive interactions on the long-term behavior of the solutions of system (2). Investigating the long-time behavior of various group patterns can help understand how some aggregations stay together for long periods of time (see for example the analytical and numerical studies of mathematical models for locust swarms [37,2]).

The relative magnitude of these social interactions is described by the sign of the jump at the origin $[K]$. In particular, $[K] > 0$ indicates that repulsion is the effective social interaction. In this case, we show that the L^∞-norm of the solution is indeed bounded for all times. Using the results from Section 3, we conclude that the solution remains smooth, therefore it exists globally in time. This corresponds to finite density aggregations, or aggregations that disperse. In the attractive case, $[K] < 0$, we show that the solution can blow up in finite time, provided the initial condition is large enough. This may correspond to aggregations collapsing into a point.

Define

$$M^+(t) = \max_{x\in\mathbb{R}} u^+(x,t),$$
$$M^-(t) = \max_{x\in\mathbb{R}} u^-(x,t),$$

and let x_M^+, $x_M^- \in \mathbb{R}$ denote the (time-dependent) locations where such maxima are achieved. Hence,

$$M^+(t) = u^+(x_M^+(t),t), \qquad M^-(t) = u^-(x_M^-(t),t),$$

and also,

$$u_x^+(x_M^+(t),t) = 0, \qquad u_x^-(x_M^-(t),t) = 0.$$

Evaluate (2a) at $(x_M^+(t),t)$ to obtain

$$\frac{d}{dt}M^+(t) = -\gamma f'(K*u)\left([K]u(x_M^+(t),t) + K^{(1)} * u(x_M^+(t),t)\right)M^+(t) - \lambda^+ M^+(t) + \lambda^- u^-(x_M^+(t),t). \quad (28)$$

Similarly, by evaluating (2b) at $(x_M^-(t),t)$ we get

$$\frac{d}{dt}M^-(t) = -\gamma f'(K*u)\left([K]u(x_M^-(t),t) + K^{(1)} * u(x_M^-(t),t)\right)M^-(t) + \lambda^+ u^+(x_M^-(t),t) - \lambda^- M^-(t). \quad (29)$$

Case $[\mathbf{K}] \geq \mathbf{0}$ (repulsion stronger than attraction). Recall that f is assumed to be non-decreasing, that is $f' \geq 0$. Also, using $u^-(x_M^+(t),t) \leq M^-(t)$, the fact that the solution is non-negative and (14), we derive from (28):

$$\begin{aligned}\frac{dM^+}{dt} &\leq -\gamma f'(K*u)(K^{(1)} * u(x_M^+(t),t))M^+(t) + \lambda^- M^-(t)\\ &\leq \gamma\|f'\|_{L^\infty}\|K^{(1)}\|_{L^\infty}\|u\|_{L^1}M^+(t) + \|\lambda^-\|_{L^\infty}M^-(t)\\ &\leq C(M^+(t) + M^-(t)),\end{aligned} \quad (30)$$

for some constant C that depends on the initial data. A similar estimate is satisfied by $M^-(t)$. By adding the two, we derive

$$\frac{d}{dt}(M^+(t) + M^-(t)) \leq C(M^+(t) + M^-(t)).$$

The Gronwall lemma guarantees that M^+ and M^- do not blow up in finite time. Therefore, u^+ and u^- remain bounded and the solution exists globally in time. This guarantees that when repulsion dominates the social interactions, the aggregations are described by finite-amplitude patterns.

Case $[\mathbf{K}] < \mathbf{0}$ (attraction stronger than repulsion). Assume that f' satisfies the additional following property:

$$(\mathrm{P4})' \qquad f'(x) \geq f'(y) \geq 0, \quad \text{when} \quad |x| \leq y.$$

This property may seem overly restrictive, but it is satisfied for instance by $f(x) = x$ (a popular choice in previous aggregation models [2,13,26,22]) or $f(x) = \tanh(x)$ (with $f'(x) = 1/\cosh^2(x)$) considered in the numerical results from Section 5.

From equation (28), using the non-negativity of the solution and $f' \geq 0$, we have

$$\begin{aligned}\frac{dM^+}{dt} &\geq -\gamma f'(K*u)[K](M^+(t))^2 - \gamma f'(K*u)(K^{(1)}*u)M^+(t) - \lambda^+ M^+(t) \\ &\geq -\gamma f'(\|K\|_{L^\infty}\|u\|_{L^1})[K](M^+(t))^2 - \left(\gamma\|f'\|_{L^\infty}\|K^{(1)}\|_{L^\infty}\|u\|_{L^1} + \|\lambda^+\|_{L^\infty}\right) M^+(t),\end{aligned}$$

where we used property $(\mathrm{P4})'$ of f for the last inequality.

Therefore, using (14) we obtain

$$\frac{dM^+}{dt} \geq \alpha(M^+)^2 - \beta M^+, \tag{31}$$

with

$$\alpha = -\gamma f'(\|K\|_{L^\infty}\|u_0\|_{L^1})[K], \qquad \beta = \gamma\|f'\|_{L^\infty}\|K^{(1)}\|_{L^\infty}\|u_0\|_{L^1} + \|\lambda^+\|_{L^\infty}. \tag{32}$$

So, if initially $M^+(0) > \frac{\beta}{\alpha}$, the solution $M^+(t)$ becomes unbounded in finite time. This follows by integrating (31) to get

$$M^+(t) \geq \frac{\beta}{\alpha}\frac{1}{1 - \frac{\beta}{\alpha M^+(0)}e^{\beta t}}.$$

Clearly, the right-hand-side becomes unbounded at

$$T = -\frac{1}{\beta}\log\left(1 - \frac{\beta}{\alpha M^+(0)}\right).$$

A similar argument can be worked out for $M^-(t)$.

We can now summarize all the results of this section in the following theorem:

Theorem 41. *Consider system (2) with non-negative initial data $(u_0^+, u_0^-) \in W^{2,1}(\mathbb{R}) \times W^{2,1}(\mathbb{R})$. We distinguish two cases:*

1. *Case $[K] > 0$ (global existence). The solution $(u^+(\cdot,t), u^-(\cdot,t))$ remains bounded for arbitrarily long times. Hence, using Therem 31, we conclude that a solution exists globally in $W^{2,1}(\mathbb{R}) \times W^{2,1}(\mathbb{R})$.*
2. *Case $[K] < 0$ (possible finite-time blow-up). Suppose f satisfies the additional property $(P4)'$ and α, β are defined by (32). If the initial data is large enough so that*

$$M^+(0) = \max_{x\in\mathbb{R}} u_0^+(x) > \frac{\beta}{\alpha}, \tag{33}$$

the amplitude of the solution blows up in finite time.
A similar statement can be made for large initial amplitudes in $u_0^-(x)$.

Remarks

1. We emphasize the fact that the discontinuity of the kernel represents the cause of mathematical blow-up in the case$[K] < 0$. Having $[K] < 0$ in (28), (29) means that the equations that govern the dynamics of $M^+(t)$, $M^-(t)$ are nonlinear (of the type $dy/dt = y^2$) and thus develop a finite-time singularity. For continuous kernels ($[K] = 0$), (28) and (29) basically behave like linear systems, as the coefficients of M^+ and M^- are bounded, and no finite-time blow-up is possible.
2. The condition (33) is only *sufficient* for finite time blow-up. It says that when attraction dominates the social interactions, the aggregations can collapse to a point, provided the initial group density is sufficiently large. As demonstrated in Section 5, this condition is not *necessary* as well. Initial conditions that violate (33) may still blow-up in finite time. The numerical results indicate that large turning rates (large a) prevent the blow-up. We further discuss this issue in the next section.

5 Numerical results and biological interpretation

We investigate numerically the patterns displayed by system (2), and compare the results with the analytical findings from the previous sections. We use a pseudospectral method for space discretization, and a fourth order Runge-Kutta algorithm to advance the solution in time. Using a Fourier method is particularly suitable for computing the convolution $K * u$ that enters the formulas for Γ^+ and Γ^-. To calculate the convolution numerically, we simply perform a multiplication in the discrete Fourier space,

$$\widehat{K * u}\,(l) = \widehat{K}(l)\,\widehat{u}(l).$$

All numerical results presented in this section are for the kernel $K(x)$ given by (5). Note that this kernel has a simple Fourier transform that can be computed exactly:

$$\widehat{K}(l) = 2il\left(\frac{q_a}{l^2+(1/s_a)^2} - \frac{q_r}{l^2+(1/s_r)^2}\right).$$

The sign of the jump of K at the origin,

$$[K] = q_r - q_a,$$

distinguishes the attraction and the repulsion dominated cases. We present numerical results for each case.

To calculate the turning rates $\lambda^{\pm}$, we have to compute first the alignment terms $y^{\pm}$ from (9). Since the integrals in (9) cannot be represented as convolutions, we resort to quadrature rules (trapezoidal, Simpson's) to approximate them. We mention here that we also used alternative finite difference schemes for space discretization (McCormack scheme, for instance), to double check the numerical results.

The initial conditions for the simulations are

$$u^+(x,0) = u^-(x,0) = Ae^{-(x/2-L/4)^2}, \quad x \in [0,L], \tag{34}$$

where A represents the amplitude of the initial condition, and L the size of the spatial domain. All numerical results presented in this section are for $A = 1$.

The functions f and g that enter the expressions (3) and (6), are given by

$$f(x) = \tanh(x)$$

and the equation (13), respectively. In (13), we take $x_0 = 2$ for all computations.

In the numerical simulations, we distinguish two types of steady patterns: spatially homogeneous steady states, where the density of the individuals is evenly distributed over the domain and aggregations cannot form, and spatially non-homogeneous steady states, where the density is concentrated in a part of the domain where the aggregation forms. In both cases, the density is constant in time.

Case $[\mathbf{K}] > \mathbf{0}$ ($q_r > q_a$, repulsion stronger than attraction)

Figure 2 shows some of the patterns obtained when repulsion is larger than attraction. We fix the values of the following parameters: $q_a = 0.8$, $q_r = 1.0$, $q_{al} = 1$, $s_a = 1.0$, $s_r = 0.5$, $s_{al} = 1.25$, $x_0 = 2$ and $\gamma = 1$, and we investigate the behavior of the solution for various turning rates.

Figure 2(a) corresponds to the case $a = 0$, $b = 0$ (zero turning rates). In the absence of turning rates, the two densities, u^+ and u^-, move right and left, respectively. As $t \to \infty$, they approach two compactly supported moving profiles with constant amplitudes and widths. The formation of such groups with sharp edges is referred to as clumping. The fact that system (2) can exhibit clumping, complements nicely the results in [22] regarding the asymptotic behavior and the steady states of an aggregation model that describes the evolution of just one population density field. Note that in [22], the authors show only stationary clumps. Here we show that such clumps can also move.

In Figures 2(b)-(d), we take $b = 0.5$ and consider 3 values for a: 0.2, 1 and 10. By increasing a we increase the random turning rates. The effect of this change can be observed in the figure as follows. The dynamics in Figure 2(b) retains some of the features from case (a) (zero turning rates), in the sense that the two profiles move right and left, respectively. However, the amplitude of the two profiles decreases in this case. Due to conservation of the total mass, the two diminishing bumps stay connected by a curve that straightens up, and the solution eventually settles into a constant spatially homogeneous steady state. When we increase a to 1 (see Figure 2(c)), we notice that the turning rates are large enough to hold the left-moving and right-moving individuals together. However, the group as a whole will disperse as the profiles decrease in a stationary fashion to a spatially homogeneous steady state. Finally, a large increase in the turning rate has a major effect on the qualitative behaviour of the solution. Namely, by making $a = 10$ (see Figure 2(d)), we obtain spatially non-homogeneous steady states, similar to the ones presented below, when attraction dominates repulsion. The finite-size stationary aggregations

obtained when the turning rates are mainly random ($a > b$) are in agreement with observations in nature, where many insect swarms (e.g., mosquito and midges swarms) are stationary or quasi-stationary, with individuals executing rapid random turnings [6,38].

To summarize, the patterns observed when $q_r > q_a$ are: 1) dispersive aggregations approaching two moving compactly supported clumps, or a spatially homogeneous steady states, and 2) stationary finite-size aggregations. Of course, our parameter domain is very large, and it is very reasonable to expect other patterns as well. We intend to make more extensive numerical investigations of this model in future work.

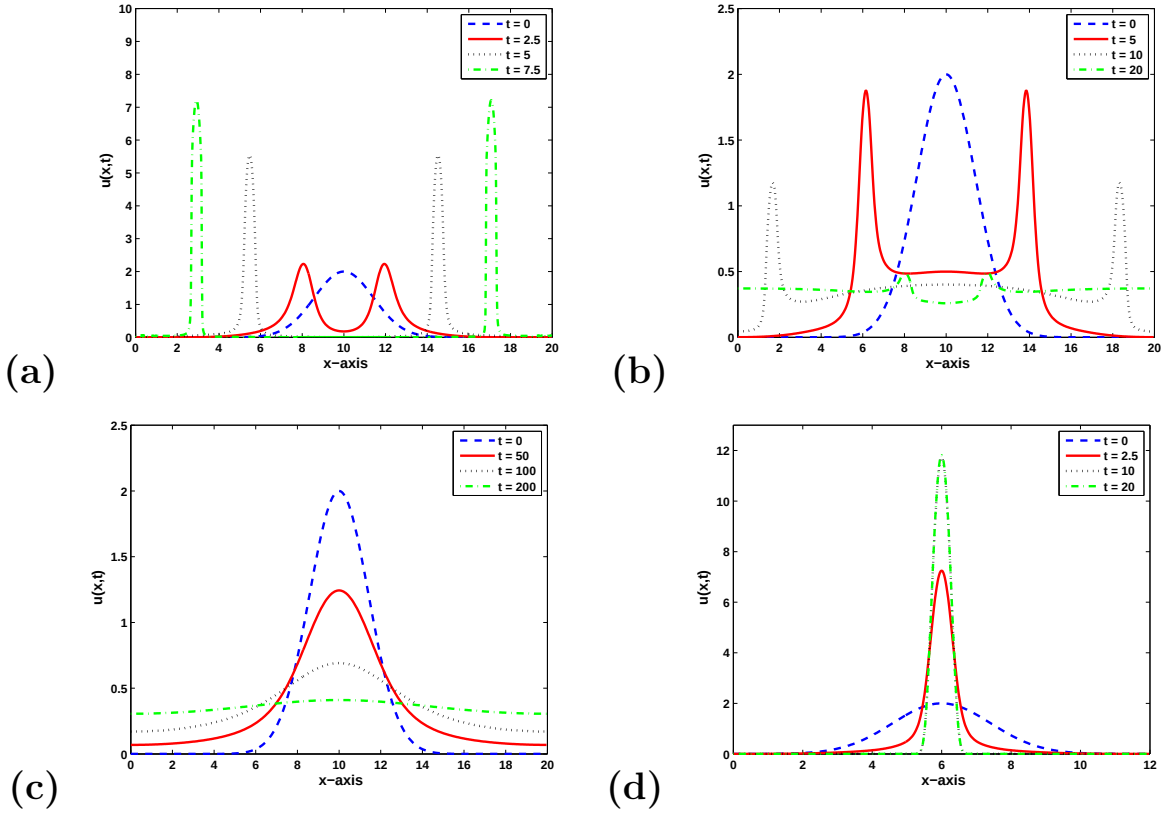

Fig. 2 Examples of patterns displayed by system (2), when $q_r > q_a$. All cases show finite-size patterns. The parameter values are as follows: (a) $a = 0$, $b = 0$ (zero turning rates); (b) $a = 0.2$, $b = 0.5$; (c) $a = 1$, $b = 0.5$; (d) $a = 10$, $b = 0.5$. In all cases, (a)-(d), the rest of the parameters are: $q_a = 0.8$, $q_r = 1$, $q_{al} = 1$, $s_a = 1$, $s_r = 0.5$, $s_{al} = 1.25$, $x_0 = 2$ and $\gamma = 1$.

Case $[\mathbf{K}] < \mathbf{0}$ ($q_a > q_r$, attraction stronger than repulsion)

Before we present the results for this case, let us revisit the inequality (33) for initial conditions that lead to finite time blow-up. For initial data (34), $\|u_0\|_{L^1} = 2\sqrt{\pi}A$, and the inequality reads

$$A > -\frac{2\sqrt{\pi}A\gamma\|f'\|_{L^\infty}\|K^{(1)}\|_{L^\infty} + a + b}{\gamma f'(2\sqrt{\pi}A\|K\|_{L^\infty})[K]}.$$

Hence, using $[K] < 0$, we can write it as

$$-f'(2\sqrt{\pi}A\|K\|_{L^\infty})[K] > 2\sqrt{\pi}\|f'\|_{L^\infty}\|K^{(1)}\|_{L^\infty} + \frac{a+b}{\gamma A}. \tag{35}$$

Note that this inequality does not hold for large turning rates a and b, or small velocity γ.

The patterns we observe in the case when attraction is larger than repulsion, range from finite-size to blow-up aggregations. The latter may correspond to very dense aggregations that collapse into a point. Figure 3 shows some of these patterns. As mentioned above, the large parameter space strongly suggests that there could be other patterns as well. In view of inequality (35), and to remain consistent with the presentation of the case $[K] > 0$, we show a few patterns that illustrate the dependence of solutions on the turning rates.

In all numerical results presented below, the initial data is (34), where $A = 1$ and $L = 12$. Note that in those cases where the solution has a very localized behaviour (such as blow-up), the figures are zoomed in to show only the region of interest.

Figure 3(a) corresponds to values of parameters that satisfy the blow-up condition (35). The graph indicates a fast blow-up of the amplitude of the solution, confirming the analytical result that (35) is *sufficient* for finite-time blow-up. The condition is not *necessary* for blow-up, however. This fact is illustrated in Figure 3(b), where a choice of parameters that violates condition (35), also leads to finite-time blow-up.

In Figures 3(b)-(d), we investigate the dependence of the solution on the turning rates, similarly to what we did for the repulsion dominated case. We keep all parameters except a and b fixed, and we consider 3 cases: (b) $a = 0.2, b = 0$, (c) $a = 1, b = 0.5$ and (d) $a = 10, b = 0.5$. Case (b) leads to blow-up, as discussed above. Note here that case (a) shows a stationary blow-up, while case (b) shows a moving blow-up. The movement seems to be caused by the nonzero turning rate a. The last two cases presented in Figure 3(c)-(d) show two spatially non-homogeneous steady-state aggregations. More precisely, Figure 3(c) shows a relatively small amplitude aggregation, with the density concentrated at the edges of the group. Figure 3(d), on the other hand, shows a high-density aggregation. Note that despite these high densities, the large random turning rates prevent the swarm from collapsing into one point (i.e., mathematical blow-up). This might explain the aggregation patterns described in insect swarms which were never observed to contract so significantly to the point of collapsing. Compared to these swarms, it seems that extremely dense aggregations can only occur in organisms where the random turning is much reduced (e.g., schools of fish [7,8]). Also note the shape of the aggregations in Figure 3(c)-(d). The groups are very well defined, with the density outside the group being essentially zero. The densities u^+ and u^- are greater at the leading edges, due to individuals turning around to return to the group. The formation of biological aggregations with sharp edges has been previously reported in both empirical studies [39,40] and numerical simulations of various mathematical models [13,16].

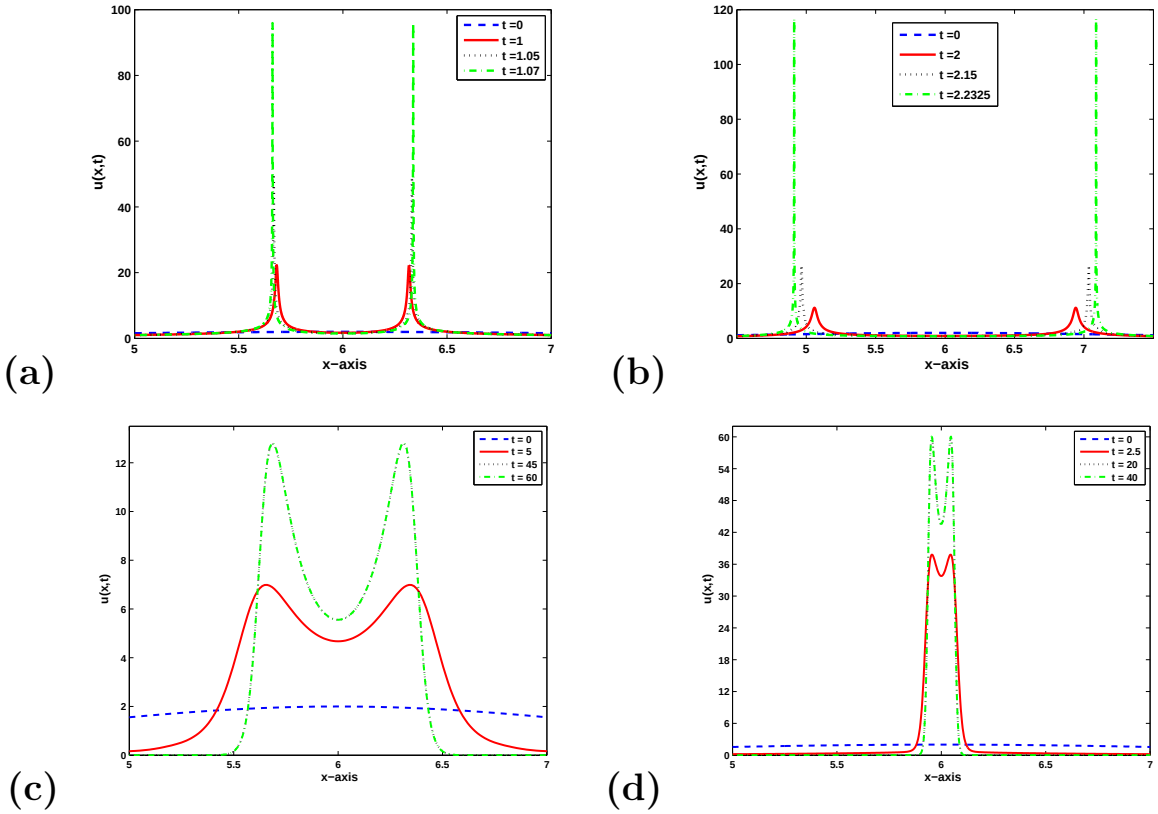

Fig. 3 Examples of patterns displayed by system (2), when $q_r < q_a$. Case (a) shows the blow-up pattern obtained when condition (35) holds. Cases (b)-(d) show the finite-size or blow-up patterns obtained when condition (35) does not hold. The parameter values are as follows: (a) $a = 0$, $b = 0$, $q_a = 1$, $q_r = 0.5$, $q_{al} = 1$, $s_a = 1$, $s_r = 0.5$, $s_{al} = 1.25$, $\gamma = 1$, $x_0 = 2$; (b) $a = 0.2, b = 0$; (c) $a = 1, b = 0.5$; (d) $a = 10, b = 0.5$. In cases (b)-(d), all parameters except a and b are the same: $q_a = 1$, $q_r = 0.8$, $q_{al} = 1$, $s_a = 1$, $s_r = 0.5$, $s_{al} = 1.25$, $\gamma = 1$, $x_0 = 2$.

Other numerical experiments: We investigated the role of the initial group density on group patterns, by increasing the amplitude A in the initial condition (34) from $A = 1$ to $A = 5$. We noted the following differences compared to the case $A = 1$. When $q_r > q_a$ and the values of the parameters are the same as in Figures 2(b)-(c), we no longer observe dispersal to a constant spatially homogeneous steady state. Because of the large initial group density, the interactions between group members are much stronger. In this case, repulsion is not enough to disperse the group. On the contrary, the group becomes even tighter, with the magnitude of the total density approaching 53.02 (when the parameters are as in Figure 2(b)) or 56.28 (when the parameters are as in Figure 2(c)). Note that for zero turning rates ($a = b = 0$), the increase in the initial data from $A = 1$ to $A = 5$ does not have any significant result on the behavior of the groups: the left-moving and right-moving groups keep distancing from each other, as observed in Figure 2(a). The results suggest that for $q_r > q_a$, increasing the amplitude of the initial data has a similar effect on the group structure as increasing the turning rates: it makes the group tighter and denser. However, for $q_r < q_a$, increasing the initial data seems to cause blow-up, in contrast with what is observed when increasing the random turning rates.

We also considered initial data (34) with smaller values for the amplitude A. We set $A = 0.2$ and the rest of the parameters the same as in the runs presented in Figures 2 and 3. When $q_r > q_a$, we observed no differences in the qualitative behavior of the solution between the two sets of runs ($A = 0.2$ and $A = 1$). For $q_a > q_r$ and zero turning rates we obtain blow-up, as in Figure 3(a). For $q_a > q_r$ and non-zero turning rates several interesting differences have been observed. In particular, when $a = 0.2$ and $b = 0$ we no longer obtain blow-up, as in Figure 3(b). Instead, the solution disperses to a constant steady state in a fashion similar to that observed in Figure 2(b) (which was obtained for $A = 1$ and $q_a < q_r$). When $a = 1$ and $b = 0.5$, we do not get a non-homogeneous steady state, as in Figure 3(c). Instead, we obtain dispersal to a homogeneous steady state, with the left and right-moving individuals staying together, as in Figure 2(c) (obtained for $A = 1$ and $q_a < q_r$). Finally, when $a = 10$ and $b = 0.5$, the solution approaches a non-homogeneous steady state, as in Figure 3(d). However, here the amplitude is much smaller: only 1.12. The differences between the two sets of results (i.e., $A = 0.2$ and $A = 1$) are due to the density of individuals that influence the nonlocal speeds. For low densities ($A = 0.2$), even when $q_a > q_r$ the group disperses if the turning rates are low too. The group can be kept together only by high turning rates.

Throughout this section, we assumed that the attraction and repulsion influence both the speed and the turning rates. In a different type of experiment, we switched off the dependence of the turning rates on repulsion and attraction (i.e., in equation (7), $y_r^{\pm}[u^+, u^-]$=$y_a^{\pm}[u^+, u^-]$=0) and took all parameters to have the same values as in the numerical experiments presented in Figures 2 and 3. We obtained solutions qualitatively similar to those depicted in Figures 2 and 3, suggesting that the model is only moderately sensitive to the dependence of turning rates on repulsion and attraction. On the other hand, the numerical results presented above show that the group patterns obtained with this model are highly sensitive to the attraction and repulsion interactions that enter the nonlocal speeds.

Bifurcation with respect to the turning rates. As shown in Figure 3, the random turning rates play a role in the transitions between high-density and extremely high-density patterns. To better see the effect of the random turning on the structure of the aggregation we design the following experiment. We keep all parameters except a fixed and we run a series of numerical experiments with a taking values in a certain interval range. Starting from $a = 0.2$, corresponding to the blow-up pattern shown in Figure 3(b), we increase slowly the value of the parameter a.

In Figure 4 we plot the *amplitude* of the pattern, $\max(u) - \min(u)$, versus the random turning rate a. The results show that there exists a bifurcation value $a_c \in (0.63, 0.64)$ such that for $a < a_c$ the group collapses into a point (blow-up solutions), while for $a > a_c$ the aggregation approaches asymptotically a spatially non-homogeneous steady-state. In the blow-up regime $a < a_c$ we plot the amplitude of the solution at a fixed time $t = 4.63$. As a approaches a_c we observe that the blow-up slows down — the larger the a, the lower the amplitude of the density at $t = 4.63$. The patterns for $a < a_c$ are similar to the one seen in Figure 3(b). Note however that the analytical result from Theorem 41 cannot be used to explain the blow-up, since (35) is not satisfied for $a \in (0.2, a_c)$. As we increase the random turning rate beyond the bifurcation value a_c, finite-size aggregations start forming. We show the amplitude of the aggregation at $t = 100$, when the solutions have reached the steady state. The patterns are similar to the ones presented in Figures 3(c) and (d). As $a > a_c$ increases, the amplitude of the steady-state aggregation increases as well — this effect was already illustrated in Figures 3(c)-(d). To conclude, these results complement the analytical findings and strongly suggest that the collapse of an aggregation can be avoided by increasing the random turning rates.

It may be possible that other parameters can influence the blow-up patterns as well, but we did not investigate this issue further. It is in fact quite difficult to explore the entire parameter space, and beyond the scope of this paper. Our purpose here was to show the role of the discontinous kernels on various types of finite and blow-up patterns and to demonstrate that animals can avoid density blow-up by changing their movement.

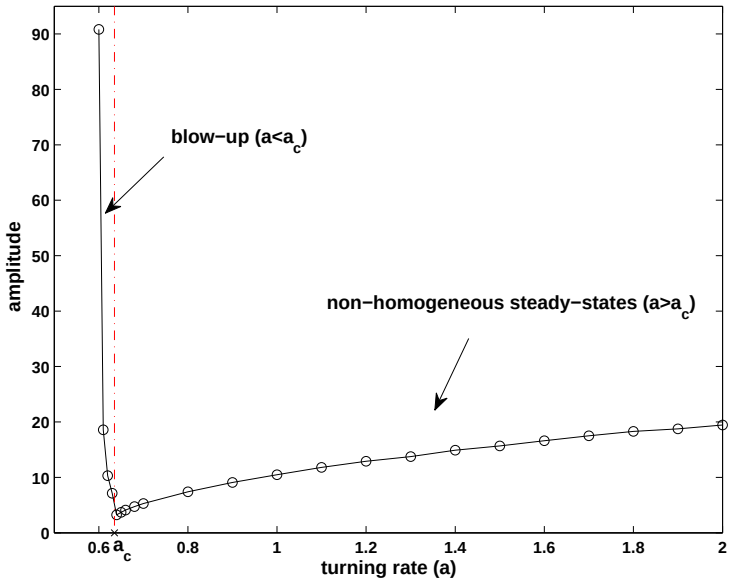

Fig. 4 Bifurcation diagram showing the amplitude of the patterns as the random turning rate a increases. There exists a bifurcation value $a_c \in (0.63, 0.64)$ such that for $a < a_c$ the solution blows up, while for $a > a_c$ the aggregation approaches asymptotically a spatially non-homogeneous steady-state, with well-defined wedges. The vertical dashed line separates the two regions. For $a < a_c$ the pattern is similar to the one in Figure 3(b). For graphical reasons, we show the amplitude of the pattern at a fixed time $t = 4.63$. Note that as a approaches a_c, the blow-up slows down — the larger the a, the lower the amplitude of the density at the specific time. For $a > a_c$ the patterns are similar to those presented in Figures 3(c) and (d). We show the solution at $t = 100$, when it has reached the steady state. We connected the points by a solid line to better indicate the amplitude trend. All parameters except a are fixed as follows: $b = 0$, $q_a = 1$, $q_r = 0.8$, $q_{al} = 1$, $s_a = 1$, $s_r = 0.5$, $s_{al} = 1.25$, $\gamma = 1$, and $x_0 = 2$.

Model (2) versus other models. Model (2) can be regarded as a generalization of existing aggregation models in two ways: i) it extends model (1) from [17,21] by introducing density-dependent velocities and ii) it extends nonlocal velocity models from papers such as [2,26,22] by including turning rates that depend on social interactions. To put our model into context, we consider system (2) with parameters having values corresponding to some of the patterns displayed in Figures 2 and 3 and perform two changes: i) switch off the dependence of velocities on the density, in order to recover system (1), and ii) take zero turning rates ($a = 0$, $b = 0$) and $f = \mathrm{Id}$, as in previous aggregation models [2,26,22].

We first discuss change i). Note that in Figures 2(c) and 3(c) the values of q_a and q_r are reversed, while all other parameter values are the same. When $q_r > q_a$ the solution disperses to a spatially homogeneous steady state, while for $q_a > q_r$ the solution approaches a spatially heterogeneous steady state. This happens for various values of q_a and q_r that are reversed. Therefore, model (2) correctly detects that attraction and repulsion have opposite effects for reversed strengths. In contrast, model (1) is not very sensitive to reversing the strengths of q_a and q_r, especially when these values are close to each other (e.g., $q_a = 0.8$, $q_r = 1$, and $q_a = 1$, $q_r = 0.8$). For instance, for model (1) both sets of parameters lead to dispersal to a spatially homogeneous steady state. Note however that model (1) is able to capture the opposite effects of the reversed strengths of q_a and q_r when these values are significantly apart from each other (e.g., $q_a = 0.1$, $q_r = 6$ and $q_a = 6$, $q_r = 0.1$).

To address change ii) we set $f = \mathrm{Id}$, $a = 0$, $b = 0$ and the attraction and repulsion parameters at the values corresponding to Figures 2 and 3(b)-(d). When repulsion dominates, $q_r = 1$ and $q_a = 0.8$, the solution approaches two right- and left-moving compactly supported profiles, very similar to what has been observed in Figure 2(a) for $f = \tanh$ and zero turning rates. If q_a and q_r are swapped, the solution blows up, in a fashion similar to the blow-up displayed in Figure 3(a). It is interesting to point out that in both experiments, the change of form of f from hyperbolic tangent to identity does not seem to affect the qualitative behavior of the solution. The solutions we obtained are consistent with the numerical results from [22] regarding the behavior of solutions to an aggregation model without alignment.

6 Discussion

In this article, we investigated the existence of different types of patterns obtained with a nonlocal hyperbolic model for self-organized animal aggregations. The model incorporates both nonlocal speeds and nonlocal turning rates that are the result of the three types of social interactions between individuals: attraction, repulsion, and alignment.

The model is able to explain some of the patterns observed in various animal groups. For example, it can explain the dispersion of an aggregation. Such a behavior can be seen in swarms of insects [6] or foraging herds of ungulates [41]. In the latter species, the repulsion dominates the attraction, and animals spread over very large areas in search for food. The model can also explain the long-time existence of finite-size groups. This behavior, which can also be seen in ungulates, is caused by large attractive interactions between the members of the group. Finally, the model can display blow-up patterns. These patterns may correspond to the collapse of some schools of fish into very tight groups [7].

Blow-up patterns have been previously obtained with local hyperbolic or parabolic models describing chemotactic behavior [19, 42]. For local hyperbolic models, these patterns are caused by the gradient of the chemical signal which influences the turning rates [19]. In this article, the mathematical blow-up arises from the discontinuity of the kernel that describes the attractive and repulsive interactions. Due to this discontinuity, the social interactions that act on extremely short ranges have a great impact on the behavior of individuals (i.e., $K(s) \neq 0$, for s close to 0). In particular, for attraction greater than repulsion, neighbors positioned at $x \pm s$ (with s close to 0) are highly attracted towards the individual positioned at x. This leads to the "pile-up" behavior which characterizes the blow-up patterns. However, this behavior cannot occur for continuous attractive and repulsive kernels $K(s)$ (e.g., kernels as in [2]). Since these kernels satisfy $K(0) = 0$, the social interactions have a very low influence on the behavior of individuals positioned at $x \pm s$, when s is small. It is likely that on such short ranges, the repulsion dominates even when attraction is greater than repulsion. It could be that animal aggregations which cannot exhibit blow-up patterns (herds of ungulates, flocks of birds) are better modeled using kernels with a small discontinuity (such as odd extensions of translated Gaussians) or even continuous kernels. An interesting direction for future work is to investigate the behavior of solutions to system (2) for various interaction kernels. The blow-up patterns displayed by our model can be either stationary or moving. Note that previous local hyperbolic models [19] were able to capture stationary blow-up patterns only. It seems that the enhanced behavior of our model is due to the presence of random turning rates.

The numerical results presented in this article suggest that the anti-crowding behavior described by the repulsive terms cannot alone lead to groups with well-defined boundaries. In this case, the groups tend to spread out (see Figures 2(b)-(c)). The formation of aggregations with well-defined boundaries requires at least one more factor, which in this paper is provided by the random turning rates. We show that moderately large turning rates can keep the group together, even when repulsion is greater than attraction. Moreover, the numerics show (see the bifurcation diagram from Figure 4) that for attraction dominated aggregations, increasing the random turning rates can prevent a group from collapsing into a point. This observation complements the analytical results regarding the possible collapse of aggregations when the turning rates and alignment interactions are small. The results suggest that the various low and high density patterns observed in nature can be explained in terms of the different turning rates that characterize the movement of organisms: large random turning rates in swarms and small random turning rates in collapsing fish schools.

In contrast with the importance of the random turning rates, the directed turning rates (and in particular the magnitude of the alignment interactions q_{al}) do not have a significant effect on the spatial and spatiotemporal patterns. Moreover, changing the attraction and repulsion forces in the turning rates has a much weaker effect on the behavior of the solution than performing a similar change in the nonlocal speeds. This is in part due to the assumption that the function g that enter the expression for the turning rates is bounded. Also interesting to point out is the fact that the particular form of the function f entering the nonlocal speeds does not seem to be so important in regard to the types of patterns that can be obtained. In particular, the hyperbolic tangent and the identity function produced similar spatial and spatiotemporal patterns.

To conclude, using a combination of numerical and analytical results, we were able to gain insight into the biological mechanisms that can explain the formation or collapse of some aggregations. The analytical results rule out the possibility of shock formation (gradient blow-up) and, depending on the case, either establish global well-posedness or predict finite-time amplitude blow-up.

Acknowledgements R.F. was supported by NSERC RGPIN-341834. R.E. acknowledges a University of Alberta Queen Elizabeth II Graduate Award and an AMI Graduate Lecture Award, which supported her research during the final year

of PhD studies at University of Alberta, in the Center for Math Biology. R.E. thanks Mark Lewis and Gerda de Vries for their valuable suggestions throughout her PhD studies.

Appendix

Local existence. We show local existence of solutions using the vanishing viscosity method. The procedure is fairly standard and we only summarize the main ideas and results.

Consider system (2) with artificial viscosity ($\nu > 0$) terms added to the right-hand-side of the equations:

$$\partial_t u_\nu^+ + \partial_x \left(\Gamma^+[u_\nu^+, u_\nu^-]u_\nu^+ \right) = -\lambda^+[u_\nu^+, u_\nu^-]u_\nu^+ + \lambda^-[u_\nu^+, u_\nu^-]u_\nu^- + \nu u_{\nu,xx}^+, \tag{36a}$$

$$\partial_t u_\nu^- - \partial_x \left(\Gamma^-[u_\nu^+, u_\nu^-]u_\nu^- \right) = \lambda^+[u_\nu^+, u_\nu^-]u_\nu^+ - \lambda^-[u_\nu^+, u_\nu^-]u_\nu^- + \nu u_{\nu,xx}^-, \tag{36b}$$

with the same initial data $u_\nu^\pm(x,0) = u_0^\pm(x)$, $x \in \mathbb{R}$.

The existence and uniqueness of a regular local solution (u_ν^+, u_ν^-) of system (36) with a smooth initial condition can be derived via the Banach fixed point theorem. The procedure is similar to that used in viscous regularizations of conservation laws and we omit the details here.

Next we show that the sequence (u_ν^+, u_ν^-) converges (on a subsequence) as $\nu \to 0$ to a solution of (2). We show that (u_ν^+, u_ν^-) satisfies the hypotheses of the Ascoli-Arzela theorem, therefore one can extract a subsequence $(u_{\nu_m}^+, u_{\nu_m}^-)$ that converges uniformly on $[0,T]\times\mathbb{R}$. It follows immediately that the limit (u^+, u^-) is a weak solution of (2). Using the a priori estimates derived in Section 3, we then conclude that u is in fact a strong solution.

Uniform L^1-estimates. These can be derived as in Section 3, as the viscosity terms are dissipative.

Uniform L^∞-estimates. Define

$$M_\nu^+(t) = \max_{x\in\mathbb{R}} u_\nu^+(x,t),$$
$$M_\nu^-(t) = \max_{x\in\mathbb{R}} u_\nu^-(x,t).$$

We derive the analogue of (28) for M_ν^+ by evaluating (36a) at the point where u_ν^+ attains its maximum. Then, using the uniform (in ν) L^1-control of $u_\nu = u_\nu^+ + u_\nu^-$, the boundedness of f', $K^{(1)}$ and g, and the fact that $u_\nu^-(\cdot,t) \le M_\nu^-(t)$, we can derive

$$\frac{d}{dt} M_\nu^+(t) \le C_1(M_\nu^+(t) + M_\nu^-(t)) + C_2(M_\nu^+(t) + M_\nu^-(t))M_\nu^+(t),$$

for some positive constants C_1 and C_2. Here we also used that at a local maximum, $u_{\nu,xx}^+$ is non-positive.

A similar inequality can be derived for $M_\nu^-(t)$. Denote

$$M_\nu(t) = M_\nu^+(t) + M_\nu^-(t),$$

and add the two inequalities to get

$$\frac{d}{dt} M_\nu(t) \le C_1 M_\nu(t) + C_2(M_\nu(t))^2,$$

for some positive constants C_1 and C_2. From this inequality one can derive

$$M_\nu(t) \le \frac{C_1}{C_2} \frac{1}{\left(1 + \frac{C_1}{C_2 M_\nu(0)}\right) e^{-C_1 t} - 1},$$

for $t < \frac{1}{C_1} \log\left(1 + \frac{C_1}{C_2 M_\nu(0)}\right)$. Therefore, by choosing a final time T such that

$$T < \frac{1}{C_1} \log\left(1 + \frac{C_1}{C_2 M_\nu(0)}\right),$$

we have

$$M_\nu(t) \le \frac{C_1}{C_2} \frac{1}{\left(1 + \frac{C_1}{C_2 M_\nu(0)}\right) e^{-C_1 T} - 1},$$

for all $t \in [0,T]$ and $\nu > 0$. This shows that there is a uniform in ν bound on $\|u_\nu^+\|_{L^\infty}$ and $\|u_\nu^-\|_{L^\infty}$ for $t \in [0,T]$.

Uniform L^∞-estimates of space derivatives. These estimates follow closely the calculations from Section 3. The smoothness of the viscosity solution legitimates the calculations. The main observation is that the L^∞-bounds of u_ν^+ and u_ν^- on $[0,T]$ are guaranteed by the previous step, while the viscous terms provide only dissipative, sign-definite quantities. For instance, take an x-derivative in (36a), multiply by $\operatorname{sgn}(u_{\nu,x}^+)$ and integrate over $\mathbb{R}$, similarly to what we did in Section 3 to derive L^1-bounds on u_x^+. Note that the viscous term yields a sign-definite quantity, as

$$\nu \int_{\mathbb{R}} u_{\nu,xxx}^+ \operatorname{sgn}(u_{\nu,x}^+) dx \le 0.$$

Therefore, using the methods from the previous section, we can derive uniform (in ν) L^1-estimates of $u_{\nu,x}^+$, $u_{\nu,x}^-$, and then uniform L^1-estimates of $u_{\nu,xx}^+$, $u_{\nu,xx}^-$. The latter imply uniform in ν estimates of $\|u_{\nu,x}^+\|_{L^\infty}$ and $\|u_{\nu,x}^-\|_{L^\infty}$.

Uniform L^∞-estimates of time derivatives. Differentiate (36a) with respect to t and set

$$w_\nu^+ = u_{\nu,t}^+, \quad w_\nu^- = u_{\nu,t}^-, \quad w_\nu = w_\nu^+ + w_\nu^-,$$

to obtain

$$w_{\nu,t}^+ + \gamma \left(f'(K*u_\nu)(K*w_\nu)u_\nu^+ + f(K*u_\nu)w_\nu^+ \right)_x = -\lambda_{\nu,t}^+ u_\nu^+ - \lambda_\nu^+ w_\nu^+ + \lambda_{\nu,t}^- u_\nu^- + \lambda_\nu^- w_\nu^- + \nu w_{\nu,xx}^+. \tag{37}$$

From (6) and (9a) we compute:

$$\lambda_{\nu,t}^+ = b\, g'(y^+) \left(q_{al} \int_0^\infty K_{al}(z)(w_\nu^-(x+z,t) - w_\nu^+(x-z,t))dz \right). \tag{38}$$

A similar formula holds for $\lambda_{\nu,t}^-$. We want to show that the solution (u_ν^+, u_ν^-) of (36) has uniformly bounded time derivatives in $[0,T]$, which is equivalent to showing that (37) (and the corresponding equation for w_ν^-) has a uniformly bounded solution (w_ν^+, w_ν^-). Using similar techniques as in Section 3, we derive a priori estimates on the L^1-norms of their 1st derivatives, $\|w_{\nu,x}^+\|_{L^1}$ and $\|w_{\nu,x}^-\|_{L^1}$, which imply the desired boundedness result. We summarize these calculations below.

We start by deriving uniform bounds on $\|w_\nu^+\|_{L^1}$ and $\|w_\nu^-\|_{L^1}$. Multiply (37) by $\operatorname{sgn}(w_\nu^+)$ and integrate over $\mathbb{R}$. The last term in the left-hand-side renders 0 and the viscous term is dissipative. We assumed that $\|f'\|_{L^\infty}$, $\|f''\|_{L^\infty}$ are bounded and we showed that $\|u_\nu^+\|_{L^\infty}$, $\|u_\nu^-\|_{L^\infty}$, $\|u_{x,\nu}^+\|_{L^\infty}$ are uniformly bounded in ν on $[0,T]$. Therefore, the second term in the left-hand-side can be estimated as follows

$$\begin{aligned}
\left| \int \left(f'(K*u_\nu)(K*w_\nu)u_\nu^+ \right)_x \operatorname{sgn}(w_\nu^+) dx \right| &\le \|f''(K*u_\nu)([K]u_\nu + K^{(1)}*u_\nu)u_\nu^+\|_{L^\infty} \|K*w_\nu\|_{L^1} \\
&+ \|f'(K*u_\nu)u_\nu^+\|_{L^\infty} \|[K]w_\nu + K^{(1)}*w_\nu\|_{L^1} + \|f'(K*u_\nu)u_{\nu,x}^+\|_{L^\infty} \|K*w_\nu\|_{L^1} \\
&\le C \left(\|w_\nu^+\|_{L^1} + \|w_\nu^-\|_{L^1} \right)
\end{aligned}$$

Note from (38) that

$$\|\lambda_{\nu,t}^+\|_{L^\infty} \le C \left(\|w_\nu^+\|_{L^1} + \|w_\nu^-\|_{L^1} \right). \tag{39}$$

A similar inequality holds for $\|\lambda_{\nu,t}^-\|_{L^\infty}$.

The right-hand-side of (37) multiplied by $\operatorname{sgn}(w_\nu^+)$ and integrated over $\mathbb{R}$ can also be easily estimated using (39), the boundedness of g and the uniform bounds on $\|u_\nu^+\|_{L^1}$ and $\|u_\nu^-\|_{L^1}$. Finally we get

$$\frac{d}{dt}\|w_\nu^+\|_{L^1} \le C \left(\|w_\nu^+\|_{L^1} + \|w_\nu^-\|_{L^1} \right).$$

A similar estimate can be derived for $\|w_\nu^-\|_{L^1}$. By adding the two and using the Gronwall's lemma, we conclude that $\|w_\nu^+\|_{L^1}$ and $\|w_\nu^-\|_{L^1}$ remain uniformly bounded on $[0,T]$.

Uniform bounds on $\|w_{\nu,x}^+\|_{L^1}$ and $\|w_{\nu,x}^-\|_{L^1}$ can be derived in a similar manner. Differentiate (37) with respect to x. The left-hand-side becomes

$$\begin{aligned}
w_{\nu,xt}^+ + \gamma \Big(& f''(K*u_\nu)([K]u_\nu + K^{(1)}*u_\nu)(K*w_\nu)u_\nu^+ + f'(K*u_\nu)([K]w_\nu + K^{(1)}*w_\nu)u_\nu^+ \\
& + f'(K*u_\nu)(K*w_\nu)u_{\nu,x}^+ + f'(K*u_\nu)([K]u_\nu + K^{(1)}*u_\nu)w_\nu^+ + f(K*u_\nu)w_{\nu,x}^+ \Big)_x
\end{aligned}$$

After multiplication by $\mathrm{sgn}(w^+_{\nu,x})$ and integration over $\mathbb{R}$, the very last term in the sum above renders 0. The first term yields

$$\frac{d}{dt}\|w^+_{\nu,x}\|_{L^1},$$

while the rest can be estimated in absolute value by

$$C\left(\|w^+_{\nu,x}\|_{L^1}+\|w^-_{\nu,x}\|_{L^1}\right). \tag{40}$$

To do this, one has to use the assumption that $\|f'\|_{L^\infty}$, $\|f''\|_{L^\infty}$, $\|f'''\|_{L^\infty}$ are bounded and the uniform bounds on $\|u^+_\nu\|_{L^\infty}$, $\|u^-_\nu\|_{L^\infty}$, $\|u^+_{\nu,x}\|_{L^\infty}$, $\|w^+_\nu\|_{L^1}$ and $\|w^-_\nu\|_{L^1}$ derived before.

Let us inspect the outcome of differentiation, multiplication by $\mathrm{sgn}(w^+_{\nu,x})$, and integration over $\mathbb{R}$ in the right-hand-side of (37). The viscous term is dissipative. The terms $\|\left(\lambda^+_\nu w^+_\nu\right)_x\|_{L^1}$ and $\|\left(\lambda^-_\nu w^-_\nu\right)_x\|_{L^1}$ can be estimated as in Section 3 (see (19) and (20)) with the upper bound given by (40). For the remaining terms we calculate $\lambda^+_{\nu,tx}$ and use the assumption that $\|g'\|_{L^\infty}$, $\|g''\|_{L^\infty}$ are bounded, together with the uniform bounds on $\|u^+_{\nu,x}\|_{L^1}$, $\|u^-_{\nu,x}\|_{L^1}$, $\|w^+_\nu\|_{L^1}$ and $\|w^-_\nu\|_{L^1}$ to derive

$$\|\lambda^+_{\nu,tx}\|_{L^\infty}\le C_1+C_2\left(\|w^+_{\nu,x}\|_{L^1}+\|w^-_{\nu,x}\|_{L^1}\right). \tag{41}$$

A similar estimate holds for $\|\lambda^-_{\nu,tx}\|_{L^\infty}$. Putting everything together, we obtain

$$\frac{d}{dt}\|w^+_{\nu,x}\|_{L^1}\le C_1+C_2\left(\|w^+_{\nu,x}\|_{L^1}+\|w^-_{\nu,x}\|_{L^1}.\right).$$

Use the similar estimate for $\frac{d}{dt}\|w^-_{\nu,x}\|_{L^1}$ and Gronwall's lemma to obtain the desired uniform in ν bounds on $\|w^+_{\nu,x}\|_{L^1}$ and $\|w^-_{\nu,x}\|_{L^1}$.

Conclusion. To conclude, due to these uniform (in ν) bounds, we can apply the Ascoli-Arzela theorem to the sequence of viscous solutions (u^+_ν,u^-_ν) and extract a subsequence $(u^+_{\nu_m},u^-_{\nu_m})$ that converges uniformly on $[0,T]\times\mathbb{R}$ to (u^+,u^-), with u^+ and u^- bounded and continuous functions. Clearly, one can pass to the limit $\nu_m\to 0$ in the weak form of (36) and conclude that (u^+,u^-) is a weak solution of (2). However, due to the various a priori estimates derived before, we can conclude that u is in fact a strong solution.

Uniqueness of a classical solution. The uniqueness of a local classical solution to (2) can also be derived from Gronwall's lemma type arguments. Suppose there exist two solutions (u^+_1,u^-_1) and (u^+_2,u^-_2) of (2) that are bounded (see (11)) in some time interval $[0,T]$. Previous considerations imply that $\|u^+_i\|_{L^1}$, $\|u^-_i\|_{L^1}$, $\|u^+_{i,x}\|_{L^1}$, $\|u^-_{i,x}\|_{L^1}$ and $\|u^+_{i,x}\|_{L^\infty}$, $\|u^-_{i,x}\|_{L^\infty}$ $(i=1,2)$ are also bounded in $[0,T]$.

Denote

$$v^+=u^+_1-u^+_2,\qquad v^-=u^-_1-u^-_2,\qquad v=v^++v^-.$$

Substract the two equations obtained by writing (2a) for u^+_1 and u^+_2 to get

$$v^+_t+\gamma v^+_x+\gamma\left(f(K*u_1)u^+_1-f(K*u_2)u^+_2\right)_x=-\lambda^+_1u^+_1+\lambda^-_1u^-_1+\lambda^+_2u^+_2-\lambda^-_2u^-_2,$$

where $u_i=u^+_i+u^-_i$ and $\lambda^\pm_i=\lambda^\pm[u^+_i,u^-_i]$, $i=1,2$. Add and substract $\gamma\left(f(K*u_1)u^+_2\right)_x$ in the left-hand-side and $\lambda^-_2u^-_1$, $\lambda^+_2u^+_1$ in the right-hand-side. Then, multiply by $\mathrm{sgn}(v^+)$ and integrate over $\mathbb{R}$. The terms γv^+_x and $\gamma\left(f(K*u_1)v^+\right)_x$ render 0 and we obtain

$$\begin{aligned}\frac{d}{dt}\|v^+\|_{L^1}\le\gamma\int\left|\left((f(K*u_1)-f(K*u_2))u^+_2\right)_x\right|dx+\int(\lambda^-_2|v^-|+\lambda^+_2|v^+|)dx\\+\int\left(|\lambda^+_2-\lambda^+_1||u^+_1|+|\lambda^-_2-\lambda^-_1||u^-_1|\right)dx.\end{aligned} \tag{42}$$

Consider the integrand of the first term in the right-hand-side. After taking the derivative we get

$$\begin{aligned}\left|\left((f(K*u_1)-f(K*u_2))u^+_2\right)_x\right|\le|f'(K*u_1)([K](u_1-u_2)+K^{(1)}*(u_1-u_2))u^+_2|\\+|(f'(K*u_1)-f'(K*u_2))([K]u_2+K^{(1)}*u_2)u^+_2|+|(f(K*u_1)-f(K*u_2))u^+_{2,x}|.\end{aligned}$$

Therefore,

$$\int \left| \Big((f(K*u_1) - f(K*u_2))u_2^+ \Big)_x \right| dx \le \|f'\|_{L^\infty} \|[K](u_1-u_2) + K^{(1)} * (u_1-u_2)\|_{L^1} \|u_2^+\|_{L^\infty}$$
$$+ \|f''\|_{L^\infty} \|K*(u_1-u_2)\|_{L^1} \|[K]u_2 + K^{(1)} * u_2\|_{L^\infty} \|u_2^+\|_{L^\infty} + \|f'\|_{L^\infty} \|K*(u_1-u_2)\|_{L^1} \|u_{2,x}^+\|_{L^\infty},$$

and hence,

$$\int \left| \Big((f(K*u_1) - f(K*u_2))u_2^+ \Big)_x \right| dx \le C\|v\|_{L^1},$$

for a constant C.

The second term in the right-hand-side of (42) can be readily bounded above by $C(\|v^+\|_{L^1} + \|v^-\|_{L^1})$ using the boundedness of λ_2^- and λ_2^+. Finally, the last term in the right-hand-side of (42) can be estimated as follows. Start from

$$\begin{aligned} |\lambda_2^+ - \lambda_1^+| &= b|g(y^+[u_2^+, u_2^-]) - g(y^+[u_1^+, u_1^-])| \\ &\le b\|g'\|_{L^\infty} |y^+[u_2^+, u_2^-] - y^+[u_1^+, u_1^-]|. \end{aligned}$$

Using (9a), we immediately derive

$$|y^+[u_2^+, u_2^-] - y^+[u_1^+, u_1^-]| \le q_{al} \left(\int_0^\infty |K_{al}(z)||v^-(x+z,t)|dz + \int_0^\infty |K_{al}(z)||v^+(x-z,t)|dz \right).$$

Combining the last two inequalities, we get

$$|\lambda_2^+ - \lambda_1^+| \le C(\|v^-\|_{L^1} + \|v^+\|_{L^1}).$$

Clearly a similar estimate holds for $|\lambda_2^- - \lambda_1^-|$, and hence, using the boundedness of $\|u_1^+\|_{L^1}$ and $\|u_1^-\|_{L^1}$, we derive

$$\int \left(|\lambda_2^+ - \lambda_1^+||u_1^+| + |\lambda_2^- - \lambda_1^-||u_1^-| \right) dx \le C(\|v^-\|_{L^1} + \|v^+\|_{L^1}).$$

After gathering the results we have

$$\frac{d}{dt}\|v^+\|_{L^1} \le C(\|v^-\|_{L^1} + \|v^+\|_{L^1}).$$

A similar result holds for v^-. By adding the two we obtain

$$\frac{d}{dt}(\|v^+\|_{L^1} + \|v^-\|_{L^1}) \le C(\|v^-\|_{L^1} + \|v^+\|_{L^1}),$$

and hence,

$$\|v^+(\cdot,t)\|_{L^1} + \|v^-(\cdot,t)\|_{L^1} \le (\|v^+(\cdot,0)\|_{L^1} + \|v^-(\cdot,0)\|_{L^1})e^{Ct}.$$

Uniqueness follows: provided the two classical solutions (u_1^+, u_1^-) and (u_2^+, u_2^-) have the same initial condition (that is, $v^+(\cdot,0) = v^-(\cdot,0) = 0$), they remain equal to each other in the time interval $[0,T]$.

The local existence and uniqueness results can be summarized in the following theorem.

Theorem 61. *(Local existence and uniqueness) Consider system (2) with non-negative initial data $(u_0^+, u_0^-) \in W^{2,1}(\mathbb{R}) \times W^{2,1}(\mathbb{R})$. Assume that the kernels K, K_{al} and the functions f, g used in defining $\Gamma^\pm$ and $\lambda^\pm$ satisfy properties (P1)-(P4) listed in Section 3. Then, there exists a $T > 0$ and a unique classical solution $(u^+(\cdot,t), u^-(\cdot,t))$ to (2) defined for $0 \le t \le T$.*

Proof The proof is basically contained in the arguments above. A local weak solution $(u^+(\cdot,t), u^-(\cdot,t))$ to (2) can be obtained via vanishing viscosity approach. The solution is obtained as a limit (in the uniform convergence norm) of a sequence of viscous solutions. As the viscous solutions are uniformly (in ν) bounded in $[0,T]$, its limit (u^+, u^-) is bounded as well. The a priori estimates guarantee that the solution remains in $W^{2,1}(\mathbb{R}) \times W^{2,1}(\mathbb{R})$. Due to the Sobolev embedding

$$W^{2,1}(\mathbb{R}) \to C_B^1(\mathbb{R}),$$

with

$$C_B^1(\mathbb{R}) = \{f \in C^1(\mathbb{R}) \text{ such that } \sup_{x\in\mathbb{R}} |f(x)| + |f'(x)| < \infty\},$$

we conclude that $(u^+(\cdot,t), u^-(\cdot,t))$ satisfies (2) in the classical sense.

Uniqueness was also proved above.

References

1. G. Gibson, Swarming behavior of the mosquito *Culex pipiens quinquefascitus*: a quantitative analysis, Physiological Entomology 10 (1985) 283–296.
2. A. Mogilner, L. Edelstein-Keshet, A non-local model for a swarm, J. Math. Biol. 38 (1999) 534–570.
3. W. K. Potts, The chorus-line hypothesis of manoeuvre coordination in avian flocks, Nature 309 (1984) 344–345.
4. I. D. Couzin, J. Krause, R. James, G. Ruxton, N. R. Franks, Collective memory and spatial sorting in animal groups, J. Theor. Biol. 218 (2002) 1–11.
5. B. L. Partridge, T. Pitcher, J. M. Cullen, J. Wilson, The three-dimensional structure of fish schools, Behav. Ecol. Sociobiol. 6 (1980) 277–288.
6. J. Downes, The swarming and mating flight of diptera, Annual Review of Entomology 14 (1969) 271–298.
7. H. R. Bullis, Observations on the feeding behavior of white-tip sharks on schooling fishes, Ecology 42 (1961) 194–195.
8. S. Springer, Some observations of the behavior of schools of fishes in the gulf of mexico and adjacent waters, Ecology 38 (1966) 166–171.
9. C. K. Hemelrijk, H. Kunz, Density distribution and size sorting in fish schools: an individual-based model, Behav. Ecol. 16 (1) (2004) 178–187.
10. E. Palsson, H. G. Othmer, A model for individual and collective cell movement in *Dictyostelium discoideum*, Proc. Natl. Acad. Sci. USA 97 (19) (2000) 10448–10453.
11. J. K. Parrish, S. V. Viscido, Traffic rules of fish schools: a review of agent-based approaches, in: C. K. Hemelrijk (Ed.), Self-organisation and evolution of social systems, Cambridge University Press, 2005.
12. F. Lutscher, Modeling alignment and movement of animals and cells, J. Math. Biol. 45 (2002) 234–260.
13. C. M. Topaz, A. L. Bertozzi, M. A. Lewis, A nonlocal continuum model for biological aggregation, Bull. Math. Bio. 68 (2006) 1601–1623.
14. P. C. Bressloff, Euclidean shift-twist symmetry in population models of self-aligning objects, SIAM J. Appl. Math. 64 (2004) 1668–1690.
15. A. Okubo, D. Grünbaum, L. Edelstein-Keshet, The dynamics of animal grouping, in: Okubo A., Levin S., Diffusion and ecological problems: modern perspectives, Springer, N.Y., 2001, pp. 197–237.
16. C. M. Topaz, A. L. Bertozzi, Swarming patterns in a two-dimensional kinematic model for biological groups, SIAM J. Appl. Math. 65 (2004) 152–174.
17. R. Eftimie, G. de Vries, M. A. Lewis, F. Lutscher, Modeling group formation and activity patterns in self-organizing collectives of individuals, Bull. Math. Biol. 69 (5) (2007) 1537–1566.
18. B. Pfistner, A one dimensional model for the swarming behavior of Myxobakteria, in: W. Alt, G. Hoffmann (Eds.), Biological Motion, Lecture Notes on Biomathematics, 89, Springer, 1990, pp. 556–563.
19. T. Hillen, A. Stevens, Hyperbolic models for chemotaxis in 1-D, Nonlinear Analysis: Real World Applications 1 (2000) 409–433.
20. F. Lutscher, A. Stevens, Emerging patterns in a hyperbolic model for locally interacting cell systems, J. Nonlinear Sci. 12 (2002) 619–640.
21. R. Eftimie, G. de Vries, M. A. Lewis, Complex spatial group patterns result from different animal communication mechanisms, Proc. Natl. Acad. Sci. 104 (17) (2007) 6974–6979.
22. A. J. Leverentz, C. M. Topaz, A. J. Bernoff, Asymptotic dynamics of attractive-repulsive swarms, SIAM J. Applied Dynamical Systems 8 (3) (2009) 880–908.
23. D. Chowdhury, K. Nishinary, A. Schadschneider, Self-organized patterns and traffic flow in colonies of organisms: from bacteria and social insects to vertebrates, Phase Transitions 77 (5) (2004) 601–624.
24. R. Eftimie, G. de Vries, M. A. Lewis, Weakly nonlinear analysis of a hyperbolic model for animal group formation, J. Math. Biol., In press. .
25. E. Buskey, J. Peterson, J. Amber, The swarming behavior of the copepod *Dioithona oculata:* in situ and laboratory studies, Limnol. Oceanogr. 41 (3) (1996) 513–521.
26. A. L. Bertozzi, J. A. Carrillo, T. Laurent, Blow-up in multidimensional aggregation equations with mildly singular interaction kernels, Nonlinearity 22 (2009) 683–710.
27. V. Gazi, K. Passino, Stability analysis of swarms, in: Proc. American Control Conf., Anchorage, Alaska, 2002, pp. 1813–1818.
28. M. Treiber, A. Hennecke, D. Helbing, Derivation, properties, and simulation of a gas-kinetic-based nonlocal traffic model, Physical Review E. 59 (1) (1999) 239–253.
29. T. Onouchi, T. Nagatani, Expansion, compression and triangular shockwaves in traffic flow above critical point, Physica A 373 (2007) 713–720.
30. Y. Tajima, T. Nagatani, Scaling behavior of crowd flow outside a hall, Physica A 292 (2000) 545–554.
31. M. Rascle, C. Ziti, Finite time blow up in some models of chemotaxis, J. Math. Biol. 33 (1995) 388–414.
32. T. Hillen, K. Painter, A user's guide to PDE models for chemotaxis, J. Math. Biol. 58 (1-2) (2009) 183–217.
33. A. Mogilner, L. Edelstein-Keshet, L. Bent, A. Spiros, Mutual interactions, potentials, and individual distance in a social aggregation, J. Math. Biol. 47 (2003) 353–389.
34. P. D. Lax, Hyperbolic systems of conservation laws and the mathematical theory of shock waves, Society for Industrial and Applied Mathematics, Philadelphia, Pa., 1973, conference Board of the Mathematical Sciences Regional Conference Series in Applied Mathematics, No. 11.
35. J. Smoller, Shock Waves and Reaction-Diffusion Equations, Vol. 258 of Grundlehren der Mathematischen Wissenschaften, Springer-Verlag, New York, 1983.
36. A. Sinclair, M. Norton-Griffiths, Serengeti: Dynamics of an ecosystem, University of Chicago Press, 1979.
37. L. Edelstein-Keshet, J. Warmough, D. Grunbaum, Do traveling band solutions describe cohesive swarms? An investigation of migratory locusts, J. Math. Biol. 36 (1998) 515–549.
38. A. Okubo, H. Chang, An analysis of the kinematics of swarming of *Anarete pritchardi* kim (diptera: Cecidomyiidae), Population Ecology 16 (1) (1974) 1–42.
39. B. Uvarov, Grasshoppers and locusts, Centre for Overseas Pest Research, London, 1966.
40. D. Bumann, J. Krause, Front individuals lead in shoals of three-spined sticklebacks (*Gasterosteus aculeatus*) and juvenile roach (*Rutilus rutilus*), Behaviour 125 (1993) 189–198.

41. P. Jarman, M. Jarman, Serengeti: Dynamics of an ecosystem, University of Chicago Press, 1979, Ch. The dynamics of ungulate social organization.
42. H. Othmer, A. Stevens, Aggregation, blowup, and collapse: The abc's of taxis in reinforced random walks, SIAM J.Appl.Math. 57 (4) (1997) 1044–1081.